of the 5′-flanking region from −2.6 kb to −271 bp had no effect on the level of transactivation by δEF1 (6.3- to 7.4-fold over the activity seen with empty vector), while deletion of the first intronic region between +43 bp and +2.7 kb augmented transactivation by δEF1 (11.4-fold with −271 to +42 bp versus 7.1-fold with −271 bp to +2.7 kb). Further deletion of the −271/−81 bp region resulted in significant reductions in δEF1-mediated reporter activity, which suggests that δEF1 affected promoter activity mainly via the proximal promoter region between −271 and +45 bp.

Within the 271-bp 5′-flanking region, there are two E boxes, a potential *cis*-element called THR (TGF-β1 hypersensitivity region [Cogan et al., 2002]), two CArG elements, and a TCE (TGF-β control element [Hautmann et al., 1997]), which are well conserved among species (Shimizu et al., 1995). Although δEF1 reportedly binds to a subset of E box sequences (Sekido et al., 1994), the *SM α-actin* E boxes do not accommodate very well the consensus binding sequence for δEF1 (CACCTG). To investigate the involvement of the E boxes, THR, CArG, and TCE in transactivation by δEF1, they were mutated within the −271/+42 bp reporter construct. Mutation of the E boxes, CArG-A, or TCE had little effect on transactivation of the promoter by δEF1 (Figure 3C). By contrast, mutation of THR or CArG-B significantly impaired promoter activation, and double mutation of THR and CArG-B further decreased the reporter activity transactivated by δEF1. THR and CArG-B thus appear to be required for transactivation of the *SM α-actin* −271/+42 bp region by δEF1.

We next analyzed the binding of δEF1 to the THR and CArG-B in vitro. In EMSAs using nuclear extract prepared from cultured SMCs, the THR probe elicited a specific band shift (Figure 3D, lane 1). This shift was partially inhibited by a cold probe for the E box (CACCTG) within the *immunoglobulin κ* enhancer (lanes 2 and 3), but it was much more efficiently inhibited by cold probe for the THR element (lanes 4 and 5). On the other hand, cold probe in which the THR element was mutated did not inhibit the band shift (lanes 6 and 7). Moreover, the band was super shifted by the addition of anti-δEF1 antibody (lane 8), confirming that the band contained δEF1. Anti-USF1 antibody did not affect the shift band. Probes containing the *SM α-actin* E boxes did not shift bands containing δEF1 (lanes 11 and 12), indicating that δEF1 binds to the THR element but not the E boxes within the *SM α-actin* proximal promoter region. It thus appears that δEF1 transactivates the *SM α-actin* promoter at least in part via binding to the THR element.

δEF1 Interacts with SRF

The results of the reporter analyses indicate that CArG-B is also required for δEF1 action. However, the CArG-B probe did not form shift bands with in vitro translated δEF1 in EMSA (data not shown), suggesting δEF1 might be involved in the activity of CArG-B via interactions with SRF. To address this possibility, we analyzed binding proteins to CArG-B by DNA affinity binding assays (Suzuki et al., 1993). When the biotinylated CArG-B probe was incubated with SMC nuclear extracts, SRF, δEF1, and Smad3 were detected in the bound proteins (Figure 3E). To test whether δEF1 requires SRF to bind CArG-B, the biotinylated CArG-B probe was incubated with in vitro translated δEF1 protein in the presence or absence of SRF. As shown in Figure 3F, δEF1 bound the CArG-B probe only when SRF was present.

To further characterize interactions between δEF1 and SRF, we carried out coimmunoprecipitation experiments with whole-cell lysates prepared from cultured SMCs (Figures 4A and 4B). When the lysates were subjected to immunoprecipitation, we detected SRF in immunoprecipitates pulled down with anti-δEF1 antibody (Figure 4A) and detected δEF1 in those pulled down with anti-SRF antibody (Figure 4B), which indicates that endogenous δEF1 protein physically interacts with SRF protein.

We then determined which domains of δEF1 and SRF interact with one another with expression vectors encoding truncated forms of δEF1 and SRF. Coimmunoprecipitation experiments showed that the two proteins interact mainly via δEF1 regions containing two zinc-finger domains and a SRF region containing a MADS box (Figures 4C and 4D).

δEF1 Cooperates with SRF and Smad3 to Activate the *SM α-actin* Promoter

Previous studies have shown that in AKR-2B fibroblasts, the reactivity of THR can vary in in vivo footprinting evoked by TGF-β (Becker et al., 2000). Moreover, Postigo recently reported that in osteoblasts δEF1 interacts with Smads, thereby playing a key role in the regulation of transcription mediated by TGF-β signaling (Postigo, 2003). These findings suggested that δEF1 might interact with Smads and play a role in TGF-β signaling in SMCs. To test that hypothesis, we first cotransfected a luciferase reporter vector containing the *SM α-actin* regulatory region (−2.6 to +2.7 kb) with vectors encoding δEF1 and Smad3 into SMCs. Subsequent reporter analyses showed synergistic activation of *SM α-actin* reporter activity by δEF1 and Smad3 (Figure S1A). Conversely, Smad7, an inhibitory Smad, suppressed transactivation of the *SM α-actin* by δEF1, lending additional support to the idea that Smads are involved in transcriptional control by δEF1 (Figure S1B). That δEF1 physically interacts with Smads was confirmed by coimmunoprecipitation experiments with whole-cell lysates of SMCs. δEF1 was detected in immunoprecipitates pulled down with anti-Smad3 antibody (Figure 5A), and Smad3 was detected in immunoprecipitates pulled down with anti-δEF1 antibody (Figure 5B).

Our coimmunoprecipitation (Figure 4), DNA affinity binding, and reporter (Figure 3) analyses showed that δEF1 interacts with SRF in SMCs. Interestingly, SRF also interacts with Smads (Qiu et al., 2003), while CArG elements are required for TGF-β-dependent activation of *SM α-actin* (Hautmann et al., 1997), which suggests that SRF is involved in TGF-β-dependent transcriptional control. Bearing that in mind, we next tested whether δEF1, SRF, and Smad3 might all interact in the transcriptional control of *SM α-actin* expression. Our reporter analyses consistently showed that overexpressing SRF in rat aortic SMCs inhibited somewhat the activity of SMC differentiation marker gene promoters, including those of *SM α-actin* and *SM-MHC*, whereas SRF transactivated those promoters in non-SMC cells, such as NIH3T3, BALB/3T3, and COS cells. Although the exact mechanism for this SMC-selective inhibition is

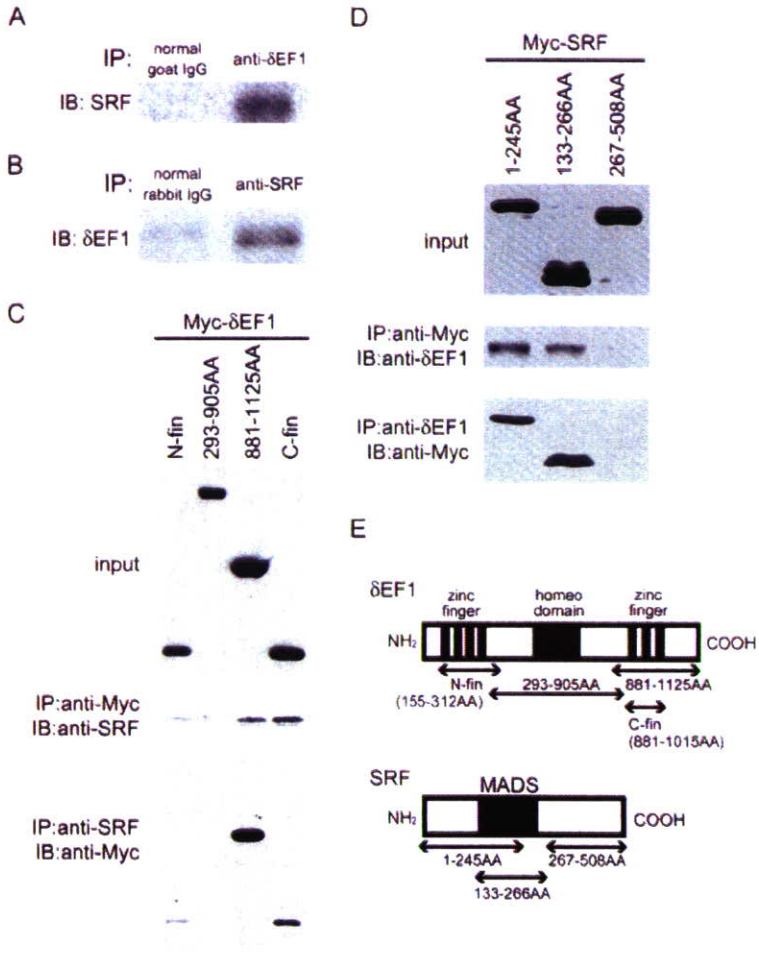

Figure 4. Interaction between δEF1 and SRF

(A and B) Physical association of δEF1 and SRF. Whole-cell lysates prepared from cultured rat aortic SMCs were incubated with anti-δEF1 antibody (A), anti-SRF antibody (B), or normal IgG (control). The reactants were immunoprecipitated with protein G (A) or anti-rabbit IgG (B) agarose-conjugated antibody, and immunoprecipitates were subjected to immunoblotting with anti-SRF antibody (A) or anti-δEF1 antibody (B).

(C and D) Analysis of the interaction between domains within δEF1 and SRF proteins. Myc-tagged δEF1 or SRF deletion constructs were transfected into cultured SMCs. Lysates of the cells were incubated with the indicated antibodies (IP), and immunoprecipitates were subjected to immunoblot with the indicated antibodies (IB).

(E) The domains are schematically illustrated.

unknown, competition for coactivators has been proposed as a possible mechanism (Prywes and Zhu, 1992). Because of this inhibitory effect of SRF, we used NIH3T3 cell in the following experiments. In those cells, SRF transactivated the full-length (−2.6 to +2.7 kb) *SM α-actin* reporter, eliciting a 13.8-fold increase in activity (Figure 5C). By themselves, Smad3 or δEF1 each only slightly increased the luciferase activity of the full-length (−2.6 to +2.7 kb) *SM α-actin* reporter (3.2-fold and 2.2-fold, respectively) (Figure 5C). Interestingly, introduction of a constitutively active form of the TGF-β type 1 receptor, caALK5, increased basal reporter activity (8.2-fold increase versus control without caALK5) (Figure 5C versus Figure 5D), and under those conditions, Smad3 and δEF1 clearly augmented transactivation of the reporter (6.4- and 5.6-fold increase over the control with caALK5), suggesting that the activities of both the *SM α-actin* promoter and δEF1 are dependent upon Smad signaling. Cotransfection of SRF and either Smad3 or δEF1 resulted in synergistic activation of the reporter activity, irrespective of the inclusion of caALK5 (Figures 5C and 5D). Moreover, cotransfection of constructs for SRF, Smad3, and δEF1 resulted in further activation of the reporter. We found similar patterns of activation of the −271/+42 bp construct (Figure S2), although overexpression of SRF increased the reporter activity to a much greater extent. Thus, SRF, δEF1, and Smad all appear to be important for *SM α-actin* transcription, and the synergistic activation observed with combinations of these transcription factors suggests that they interact to control promoter activity.

δEF1 Is Involved in TGF-β-Dependent Transcriptional Control of *SM α-actin*

The involvement of δEF1 in Smad3-dependent transcriptional control in SMCs suggests that δEF1 may be required for TGF-β-induced *SM α-actin* transcription. To test this idea, we first examined TGF-β-evoked δEF1 expression. Levels of δEF1 protein were increased by TGF-β stimulation, peaking within 12 hr and then returning to baseline within 24 hr (Figure 5E). Levels of δEF1 mRNA were also increased by TGF-β (Figure 5G).

We then analyzed the effect of δEF1 knockdown with siRNA (Figures 5F and 5G). δEF1-siRNA or a control-scrambled siRNA was transfected into cultured SMCs, after which the cells were stimulated with TGF-β. δEF1-siRNA successfully knocked down expression of δEF1 at both the mRNA (Figure 5F) and protein (Figure 5G) levels. In cells transfected with control siRNA, TGF-β induced δEF1 expression that peaked within 4 hr after stimulation (Figure 5G). In those cells, SM α-actin expression was clearly increased within 4 hr and peaked within 8 hr after TGF-β stimulation. In cells transfected with δEF1-siRNA, by contrast, the TGF-β-induced

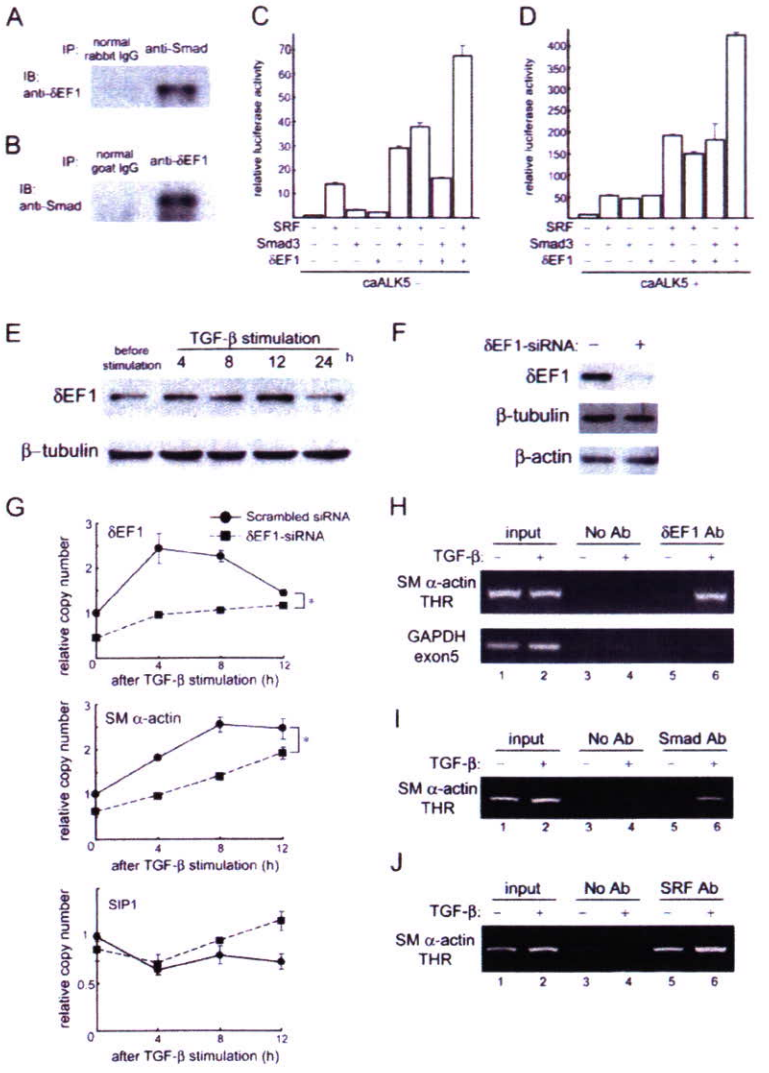

Figure 5. δEF1 in TGF-β Signaling

(A and B) Physical association between Smad and δEF1. SMC lysates were incubated with the indicated antibodies (IP) and immunoprecipitated. δEF1 (A) or Smad3 (B) in the immunoprecipitate was detected with the corresponding antibodies.

(C and D) Effects of SRF, Smad3, and δEF1 on the *SM α-actin* promoter. NIH3T3 cells were cotransfected with full-length *SM α-actin* luciferase plasmid and expression vectors encoding SRF, Smad3, and/or δEF1, with or without constitutively active ALK5 (caALK5), as indicated. The luciferase activity was normalized to that of the *SM α-actin* reporter cotransfected with empty plasmid. Bars indicate relative luciferase activity and SE.

(E) Induction of δEF1 protein by TGF-β stimulation. Rat aortic SMCs were cultured in serum-free defined medium for 4 days, after which TGF-β (2.5 ng/ml) was added to the medium. Whole-cell lysates were subjected to Western analyses of δEF1 and β-tubulin.

(F) Cells transfected with either δEF1-siRNA or control siRNA and incubated in serum-free medium for 24 hr were harvested, after which their whole-cell lysates were subjected to Western analyses.

(G) Effects of δEF1 knockdown on *SM α-actin* expression. Either δEF1-specific siRNA or control scrambled siRNA was transfected into SMCs. Twenty-four hours later, the medium was changed to serum-free defined medium for an additional 24 hr, after which TGF-β (2.5 ng/ml) was added for the indicated times. mRNA expression was analyzed by real-time PCR. Solid lines represent gene expression in cells transfected with the scrambled siRNA; dotted lines, expression in cells transfected with δEF1-siRNA. Error bars represent SE from triplicate culture wells; *$p < 0.05$ (two-way ANOVA).

(H–J) ChIP analysis of δEF1, SRF, and Smad3 binding to the endogenous *SM α-actin* promoter region containing the THR under TGF-β1 stimulation. SMCs were cultured in defined serum-free medium for 4 days and then treated with TGF-β1 (2.5 ng/ml) for 12 hr. Chromatin samples prepared from these cells were subjected to ChIP analysis. PCR was carried out to detect the *SM α-actin* promoter. Lanes 1 and 2 show amplification of total input DNA. Lanes 3 and 4 show PCR amplification of control samples precipitated with no antibody. Lanes 5 and 6 show amplification of target sequences within the immunoprecipitates. The sequence of GAPDH, which does not contain a δEF1 binding sequence, was also amplified to confirm the specificity of the assay (H).

upregulation of δEF1 was clearly suppressed (Figure 5G), as were the level of SM α-actin expression at 0 hr and its subsequent upregulation. Thus, knocking down δEF1 in SMCs attenuated the upregulation of SM α-actin otherwise seen following TGF-β stimulation, indicating δEF1 plays an important role in the TGF-β-dependent transcriptional control of *SM α-actin* expression. In addition, we also found that knocking down Smad3 resulted in inhibition of *SM α-actin* expression (Figure S3).

To confirm that endogenous δEF1, SRF, and Smad bind to the endogenous *SM α-actin* promoter in intact chromatin, cross-linked chromatin samples prepared from SMCs were subjected to chromatin immunoprecipitation (ChIP) assays. The *SM α-actin* promoter region was pulled down with antibodies against δEF1 or Smad3 in SMCs treated with TGF-β1 (Figures 5H and 5I) but was almost undetectable in the precipitants of untreated cells. The binding of SRF to the promoter was also augmented by TGF-β stimulation (Figure 5J). Clearly, TGF-β stimulation induces binding of δEF1, Smad3, and SRF to the endogenous *SM α-actin* promoter.

δEF1 Plays a Role in SMC Differentiation In Vivo

We then examined the in vivo expression of SMC differentiation marker genes in the aortas of *δEF1* knockout mice (Figure 6). We observed no apparent gross abnormalities in the cardiovascular systems of either $\delta EF1^{-/-}$ or $\delta EF1^{+/-}$ mice. Given the lethality of the $\delta EF1^{-/-}$ genotype, we decided to examine expression of SMC differentiation marker genes in aortas collected from embryos on E18.5. Using real-time PCR, we found that the levels of expression of SM α-actin, SM22α, and SM-MHC were lower in both $\delta EF1^{-/-}$ and $\delta EF1^{+/-}$ embryos than in wild-type embryos (Figures 6C–6F), while expression of

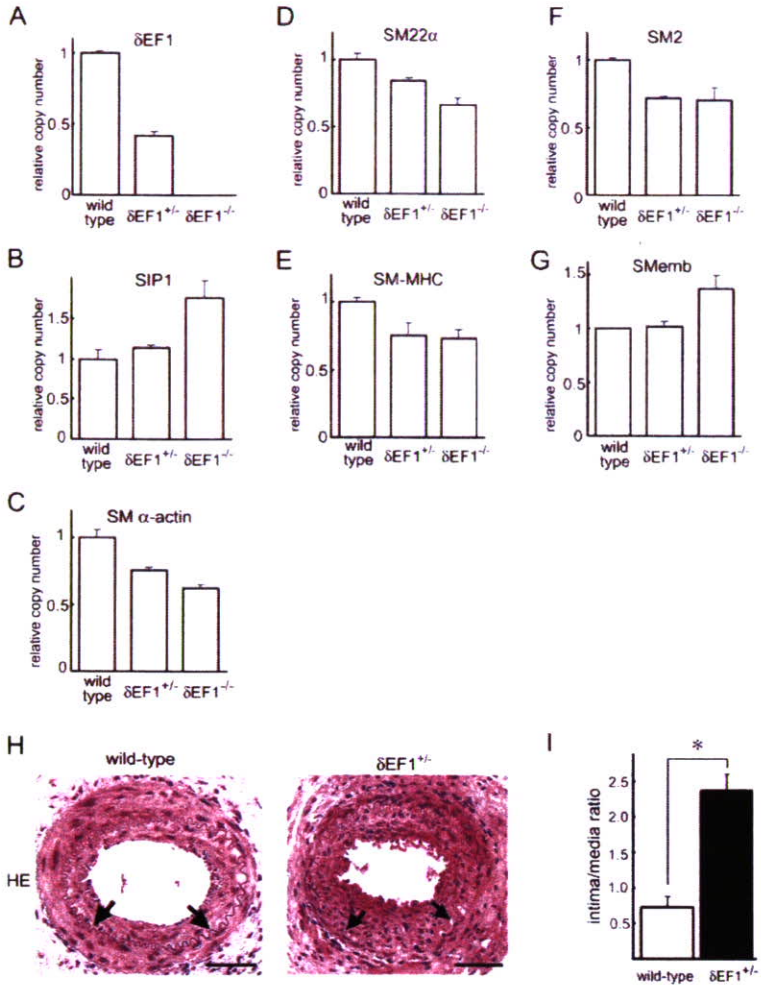

Figure 6. Effects of Haploinsufficiency of *δEF1* on Vascular Lesion Formation

(A–G) Real-time PCR analysis of the expression of δEF1, SIP1, and SMC markers in the aortas of wild-type, $\delta EF1^{+/-}$, and $\delta EF1^{-/-}$ embryos. Aortas were collected from embryos of each genotype (n = 3, 4, and 3, respectively), after which total RNA was isolated from the collected samples, and real-time PCR was carried out. The relative numbers of transcripts were normalized to those of 18S, after which expression of the transcript for each genotype was further normalized to that of the wild-type embryo. Error bars represent SE in real-time PCR data.

(H) Representative photomicrographs of transverse sections of femoral arteries harvested from wild-type and $\delta EF1^{+/-}$ mice 4 weeks after injury with a catheter guide wire. The sections were stained with hematoxylin-eosin.

(I) Neointimal/medial wall area ratios; bars are means ± SE; n = 4 for each genotype.

SMemb was higher in $\delta EF1^{-/-}$ embryos than in wild-type or $\delta EF1^{+/-}$ embryos (Figure 6G).

It was interesting to us that although aortic SMCs from $\delta EF1^{-/-}$ embryos exhibited retarded differentiation on E18.5, SMC differentiation marker genes were still expressed in $\delta EF1^{-/-}$ embryos, albeit at a lower level. In that regard, SIP1/ZEB-2, a transcription factor closely related to δEF1, was expressed in the aortas of E18.5 embryos and adult mice, and its expression was higher in $\delta EF1^{-/-}$ than in wild-type embryos (Figure 6B), suggesting that SIP1 might have acted to compensate for the lack of δEF1 function in the knockout mice (see Discussion).

$\delta EF1^{+/-}$ mice do not exhibit a clearly abnormal arterial phenotype, but we hypothesized that injury might elicit abnormal responses, as has been seen when other transcription factor genes were targeted (Manabe and Nagai, 2003). Moreover, previous studies have demonstrated that alteration of the differentiated state of SMCs plays an important role in vascular lesion formation and that changes in the course of phenotypic modulation and redifferentiation of SMCs during lesion formation may affect the outcome after vascular injury (Owens et al., 2004; Wiegman et al., 2000). With that in mind, we carried out vascular injury experiments in $\delta EF1^{+/-}$ knockout mice in which the femoral arteries were injured by using catheter guide wires. In $\delta EF1^{+/-}$ mice, neointimal lesions observed 4 weeks after the injury were much more prominent than in wild-type mice (Figure 6H), leading to significantly ($p < 0.001$) higher intimal/medial area ratios in $\delta EF1^{+/-}$ mice (Figure 6I). Moreover, as expected, we found much reduced expression of SM α-actin and SM-MHC proteins in the lesions of $\delta EF1^{+/-}$ mice (Figure S4), indicating redifferentiation of SMCs was disrupted in those animals. By contrast, we did not find clear differences in the numbers of $CD45^+$ leukocytes within the lesions.

δEF1 Is Involved in Controlling the Differentiated State of SMCs during Neointima Formation In Vivo

We further analyzed the role played by δEF1 in vascular pathology with a rat vascular injury model that enabled analysis of gene expression and SMC phenotypes. The left common carotid arteries of rats were subjected to balloon injury, after which an adenoviral vector encoding δEF1 (Ad-δEF1) or empty adenovirus was injected into the lumens of the injured arteries to infect mural cells. As evident from arteries exposed to empty adenovirus, expression of endogenous δEF1 protein was barely detectable in neointimal cells except those located adjacent to the tunica media (Figures 7Ac). The neointimal cells in the arteries exposed to empty adenovirus also

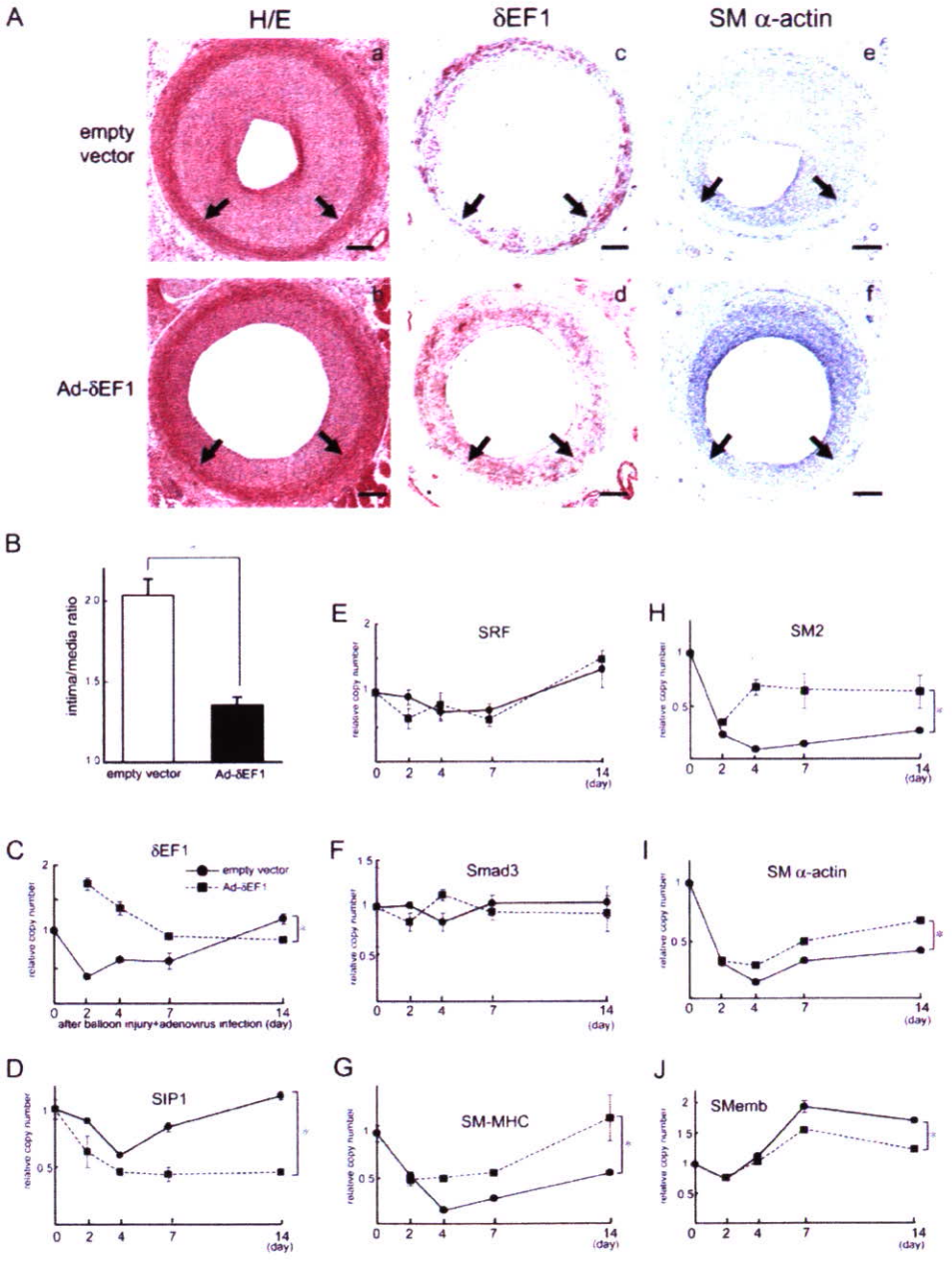

Figure 7. Effects of Adenoviral Overexpression of δEF1 on Vascular Injury Responses

(A) Representative photomicrographs of transverse sections of rat common carotid arteries harvested 2 weeks after balloon injury and injection of empty adenoviral vector (Aa, Ac, and Ae) or Ad-δEF1 (Ab, Ad, and Af). (Aa and Ab) The sections were stained with hematoxylin-eosin. (Ac and Ad) Immunohistochemical staining of δEF1 protein (red). (Ae and Af) Immunohistochemical staining of SM α-actin protein (blue). Nuclei were counterstained with nuclear fast red. Arrows indicate the internal elastic laminae. Scale bars represent 100 μm.

(B) Neointimal/medial wall area ratios; bars are means ± SE; n = 8 for each group.

(C–J) Real-time PCR analysis of mRNA expression. Solid lines represent mRNA expression in arteries infected with empty adenovirus; dotted lines, expression in arteries infected with Ad-δEF1; n = 3 in each group. Copy number of each transcript was normalized to that of 18S, after which the expression was further normalized to that in arteries without balloon injury and adenovirus injection. Graphs indicate relative copy number and SE; *p < 0.05 (two-way ANOVA).

exhibited weaker staining for SM α-actin than was seen in medial SMCs (Figure 7Ae), indicating that the neointimal cells were phenotypically modulated. Downregulation of δEF1 was also seen at the mRNA level (Figure 7C).

Ad-δEF1 infection markedly attenuated neointima formation (Figure 7Aa versus 7Ab), so that neointimal/medial wall area ratios were significantly ($p < 0.001$) lower in arteries infected with Ad-δEF1 than in those infected with empty adenovirus (Figure 7B). In the Ad-δEF1-infected arteries, δEF1 was detected in both the media and the neointima, and similar levels of SM α-actin staining were detected in medial and neointimal cells (Figure 7A). This suggests that at this point in time, neointimal cells in the Ad-δEF1-treated arteries exhibit a more

differentiated phenotype than those in arteries treated with empty adenovirus.

We then analyzed mRNA expression in the injured carotid arteries (Figures 7C–7J) and found that in arteries infected with empty adenovirus, levels of δEF1 transcript were clearly diminished by day 2 after injury and gradually returning to baseline by day 14 (Figure 7C). This reduction in δEF1 expression was accompanied by reductions in SM-MHC and SM α-actin expression (Figures 7G–7I). In the Ad-δEF1-infected arteries, by contrast, overexpression of δEF1 was observed until day 7, and the level of suppression of SM-MHC and SM α-actin was much attenuated (Figures 7G–7I). Expression of SMemb, which was induced by injury, was moderately, but significantly, decreased in the arteries infected with Ad-δEF1 (Figure 7J). Thus, judging from the observed expression of SMC phenotype marker genes, SMCs in Ad-δEF1-infected arteries are in a more differentiated state than those in control arteries. We also analyzed expression of other transcription factors. Interestingly, overexpression of δEF1 resulted in a reduction in SIP1 expression (Figure 7D), whereas expression levels of the δEF1 partners, SRF and Smad3, were not significantly affected by Ad-δEF1 infection (Figures 7E and 7F).

Discussion

One of the major findings of the present study is that δEF1 promotes the expression of SMC differentiation marker genes. δEF1 expression was upregulated during SMC differentiation of A404 cells (Figure 1C) and in mouse aorta (Figure 1D). δEF1 transactivated promoters of the SMC differentiation marker genes (Figure 2A) and upregulated expression of endogenous *SM-MHC* and *SM α-actin* in cultured SMCs (Figures 2B–2E). Moreover, knockdown of δEF1 resulted in inhibition of SM α-actin and SM-MHC induction during SMC differentiation of A404 cells (Figures 2H and 2I). Taken together, these findings demonstrate that δEF1 expression is regulated during vascular development and that, once expressed, δEF1 controls expression of various SMC differentiation marker genes and is thus actively involved in SMC differentiation. The role of δEF1 in the control of SMC differentiation was indicated further by the observations that differentiation of aortic SMCs was delayed in δEF1 knockout mice (Figure 6 and Figure S4) and that differentiation is promoted by δEF1 overexpression in cultured SMCs (Figure 2) and in injured arteries (Figure 7).

Another major finding of the present study is the involvement of δEF1 in TGF-β-dependent SMC transcriptional programs. TGF-β is thought to be one of the most important environmental cues controlling SMC differentiation (Owens et al., 2004), but little was known about how TGF-β affects the molecular machinery of SMC transcriptional programs. We were able to show in the present study (1) that δEF1 expression is regulated by TGF-β (Figure 5E); (2) that δEF1 physically interacts with Smad3 to synergistically enhance *SM α-actin* reporter activity (Figures 5A–5D); (3) that δEF1 also physically interacts with SRF (Figure 4); (4) that TGF-β induces binding of δEF1, SRF, and Smad3 to the endogenous *SM α-actin* promoter region (Figures 5H–5J); and (5) that knocking down δEF1 reduces TGF-β-induced upregulation of endogenous *SM α-actin* expression in SMCs (Figure 5G). Collectively, then, our findings suggest that δEF1 mediates TGF-β signaling by binding to both SRF and Smad3, which is consistent with earlier observations showing that CArG elements are indispensable for TGF-β-dependent transcriptional activation. Although further studies are needed to confirm whether δEF1 forms multiprotein complexes (enhanceosomes) by simultaneously binding SRF, Smad3, and other factors on the *SM α-actin* promoter, the results of the present study provide compelling evidence for the involvement of δEF1 in TGF-β-dependent SMC-specific transcriptional regulation mediated by SRF and Smad.

The finding of an interaction between δEF1 and SRF provides insight into SMC transcriptional regulatory programs that need to respond to diverse environmental cues (Owens et al., 2004). Identification of a number of the factors that interact with SRF has led to the hypothesis that protein-DNA complexes comprised of multiple factors control SMC-specific gene regulation (Miano, 2003; Owens et al., 2004). Recently, a coactivator called myocardin was reported to be specifically expressed in SMCs and cardiomyocytes and to dramatically activate SRF-dependent SMC promoters, suggesting it may be myocardin that determines the SMC-specificity of the SRF-dependent transcriptional programs. On the other hand, myocardin, alone, does not appear to be sufficient to control SMC transcriptional programs in response to diverse environmental cues (Parmacek, 2004; Pipes et al., 2005). δEF1 is interesting in this regard, as it is selectively expressed in vascular SMCs, is regulated by TGF-β, and interacts with both SRF and Smad. δEF1 thus possesses several characteristics necessary to mediate context-dependent combinatorial regulation of SMC genes. Future studies will be needed to address the role of myocardin in δEF1-mediated transcriptional control.

The attenuated expression of SMC differentiation marker genes in the aorta of $\delta EF1^{-/-}$ mice is indicative of delayed SMC differentiation there. Still, although the level was reduced, some expression of SMC differentiation marker genes did occur in $\delta EF1^{-/-}$ mice, and despite the lethality of the genotype, there were no clear morphological abnormalities within their cardiovascular systems. One possible reason for the mildness of the phenotype is that the loss of δEF1 is compensated for by other factors. Indeed, SIP1/ZEB-2, a closely related transcription factor, is also expressed in the aorta, and the level of its expression was higher in $\delta EF1^{-/-}$ mice than in wild-type mice (Figure 6B). This is consistent with earlier studies showing that $\delta EF1^{-/-}$ mice exhibit no clear phenotype in the central nervous system, skeletal muscle, or heart, where both δEF1 and SIP1 are expressed (Postigo and Dean, 2000; Takagi et al., 1998). δEF1 and SIP1 bind to similar sequences, and we found that SIP1 is also capable of transactivating SMC differentiation marker gene promoters (G.N. and I.M., unpublished data). That said, it was recently shown that δEF1 and SIP1 have distinctly different functions under certain conditions (Postigo et al., 2003), so further studies will be required to clarify the functional relationship between δEF1 and SIP1.

Finally, we found that expression of δEF1 is downregulated in neointimal SMCs (Figure 7A) and in rat carotid

arteries during the first week after balloon injury (Figure 7C) and that expression of SM α-actin, SM1, and SM2 is also downregulated during the same period (Figures 7G–7I). In addition, overexpression of δEF1 in injured arteries significantly reduced neointima formation (Figure 7B), whereas neointimal areas were significantly larger in the injured arteries of *δEF1*$^{+/-}$ mice than in those of wild-type animals (Figure 6I). The precise mechanism by which δEF1 expression affects neointima formation is not yet clear, but there are several possibilities. First, activation of differentiation programs by δEF1 may affect SMC proliferation, as differentiation and proliferation are inversely correlated in many cell types. Indeed, proliferating SMCs in vascular diseases are known to exhibit modulated phenotypes characterized by downregulation of the SMC differentiation marker genes and upregulation of *SMemb* (Manabe and Nagai, 2003). Gene expression patterns of δEF1-treated arteries and *δEF1*$^{+/-}$ animals suggest that δEF1 inhibits phenotypic modulation and/or promotes differentiation of SMCs (Figure 7 and Figure S4). It has also been shown that transcription factors that control differentiation programs directly affect cell-cycle proteins and vice versa. In that regard, TGF-β is known to control SMC proliferation in a context-dependent manner, and Postigo recently showed that δEF1 acts synergistically with TGF-β to arrest proliferation of Mv1Lu epithelial cells (Postigo, 2003). Second, in addition to contractile protein genes, δEF1 may regulate genes involved in other functions of SMCs. Neointima formation is a complex process, in which SMCs migrate, proliferate, and produce extracellular matrices and paracrine factors, thereby mediating tissue remodeling. The clear suppression of neointima formation by adenovirus-mediated δEF1 expression suggests that δEF1 may modulate various functions of SMCs in that process. In that regard, it was recently reported that δEF1 controls *collagen type 1* expression in the A7r5 cultured SMC line (Ponticos et al., 2004), which is noteworthy because collagen fibers and other extracellular matrix proteins and matrix proteases are known to affect SMC function and the pathology of blood vessels. However, we did not find that Ad-δEF1 infection significantly affected collagen deposition in the injured carotid arteries (G.N. and I.M., unpublished data). It would be important to identify additional δEF1 target genes to further clarify its role in neointima formation.

δEF1 is among only a few transcription factors that have been shown to affect neointima formation after vascular injury (Perlman et al., 1998). This suggests that modulation of δEF1 function may represent a strategy for treating vascular conditions such as the restenosis that can occur after percutaneous coronary intervention, as well as unstable plaque. Moreover, definition of the transcription factor networks of which δEF1 is one component could reveal additional potential targets for therapeutic intervention in the treatment of vascular disease.

Experimental Procedures

Plasmids

ZEB-1 constructs were kindly provided by Dr. D.C. Dean, Smad3 and ALK5 constructs were by Dr. K. Miyazono, and *SM-MHC* and *SM α-actin* reporter constructs were by Dr. G.K. Owens.

Animal Models

All animal procedures strictly adhered to the guidelines for animal experiments of the University of Tokyo.

Chromatin Immunoprecipitation

Confluent SMCs were maintained in serum-free medium for 4 days, after which TGF-β1 (2.5 ng/ml) was added to the medium. After incubating for an additional 12 hr in the presence of TGF-β1, the cells were fixed and harvested, and the samples were subjected to chromatin immunoprecipitation (ChIP) assays (Manabe and Owens, 2001a). An enhanced Supplemental Experimental Procedures section is available online.

Supplemental Data

Supplemental data include an enhanced Experimental Procedures section and supplemental figures and are available at http://www.developmentalcell.com/cgi/content/full/11/1/93/DC1/.

Acknowledgments

We gratefully acknowledge Eriko Magoshi, Noriko Yamanaka, and Michiko Hayashi for their excellent technical assistance. This study was supported in part by Grants-in-Aid from the Ministry of Education, Culture, Sports, Science and Technology, Japan (to I.M. and R.N.) and research grants from the Japan Cardiovascular Research Foundation, the Japan Vascular Disease Research Foundation, and Takeda Science Foundation (to I.M.).

Received: January 11, 2005
Revised: March 21, 2006
Accepted: May 10, 2006
Published: July 10, 2006

References

Becker, N.A., Kelm, R.J., Vrana, J.A., Getz, M.J., and Maher, L.J. (2000). Altered sensitivity to single-strand-specific reagents associated with the genomic vascular smooth muscle α-actin promoter during myofibroblast differentiation. J. Biol. Chem. *275*, 15384–15391.

Cogan, J.G., Subramanian, S.V., Polikandriotis, J.A., Kelm, R.J., and Strauch, A.R. (2002). Vascular smooth muscle α-actin gene transcription during myofibroblast differentiation requires Sp1/3 protein binding proximal to the MCAT enhancer. J. Biol. Chem. *277*, 36433–36442.

Dickson, M.C., Martin, J.S., Cousins, F.M., Kulkarni, A.B., Karlsson, S., and Akhurst, R.J. (1995). Defective haematopoiesis and vasculogenesis in transforming growth factor-β1 knock out mice. Development *121*, 1845–1854.

Funahashi, J., Sekido, R., Murai, K., Kamachi, Y., and Kondoh, H. (1993). δ-crystallin enhancer binding protein δEF1 is a zinc finger-homeodomain protein implicated in postgastrulation embryogenesis. Development *119*, 433–446.

Hautmann, M.B., Madsen, C.S., and Owens, G.K. (1997). A transforming growth factor β (TGFβ) control element drives TGFβ-induced stimulation of smooth muscle α-actin gene expression in concert with two CArG elements. J. Biol. Chem. *272*, 10948–10956.

Li, D.Y., Sorensen, L.K., Brooke, B.S., Urness, L.D., Davis, E.C., Taylor, D.G., Boak, B.B., and Wendel, D.P. (1999). Defective angiogenesis in mice lacking endoglin. Science *284*, 1534–1537.

Majesky, M.W. (2003). Vascular smooth muscle diversity. Curr. Atheroscler. Rep. *5*, 208–213.

Mallat, Z., Gojova, A., Marchiol-Fournigault, C., Esposito, B., Kamate, C., Merval, R., Fradelizi, D., and Tedgui, A. (2001). Inhibition of transforming growth factor-β signaling accelerates atherosclerosis and induces an unstable plaque phenotype in mice. Circ. Res. *89*, 930–934.

Manabe, I., and Owens, G.K. (2001a). CArG elements control smooth muscle subtype-specific expression of smooth muscle myosin in vivo. J. Clin. Invest. *107*, 823–834.

Manabe, I., and Owens, G.K. (2001b). Recruitment of serum response factor and hyperacetylation of histones at smooth muscle-specific

regulatory regions during differentiation of a novel P19-derived in vitro smooth muscle differentiation system. Circ. Res. *88*, 1127–1134.

Manabe, I., and Nagai, R. (2003). Regulation of smooth muscle phenotype. Curr. Atheroscler. Rep. *5*, 214–222.

Miano, J.M. (2003). Serum response factor. J. Mol. Cell. Cardiol. *35*, 577–593.

Oshima, M., Oshima, H., and Taketo, M.M. (1996). TGF-β receptor type II deficiency results in defects of yolk sac hematopoiesis and vasculogenesis. Dev. Biol. *179*, 297–302.

Owens, G.K., Kumar, M.S., and Wamhoff, B.R. (2004). Molecular regulation of vascular smooth muscle cell differentiation in development and disease. Physiol. Rev. *84*, 767–801.

Parmacek, M.S. (2004). Myocardin—not quite MyoD. Arterioscler. Thromb. Vasc. Biol. *24*, 1535–1537.

Perlman, H., Suzuki, E., Simonson, M., Smith, R.C., and Walsh, K. (1998). GATA-6 induces p21(Cip1) expression and G1 cell cycle arrest. J. Biol. Chem. *273*, 13713–13718.

Pipes, G.C., Sinha, S., Qi, X., Zhu, C.H., Gallardo, T.D., Shelton, J., Creemers, E.E., Sutherland, L., Richardson, J.A., Garry, D.J., et al. (2005). Stem cells and their derivatives can bypass the requirement of myocardin for smooth muscle gene expression. Dev. Biol. *288*, 502–513.

Ponticos, M., Partridge, T., Black, C.M., Abraham, D.J., and Bou-Gharios, G. (2004). Regulation of collagen type I in vascular smooth muscle cells by competition between Nkx2.5 and δEF1/ZEB1. Mol. Cell. Biol. *24*, 6151–6161.

Postigo, A.A. (2003). Opposing functions of ZEB proteins in the regulation of the TGFβ/BMP signaling pathway. EMBO J. *22*, 2443–2452.

Postigo, A.A., and Dean, D.C. (1997). ZEB, a vertebrate homolog of *Drosophila* Zfh-1, is a negative regulator of muscle differentiation. EMBO J. *16*, 3935–3943.

Postigo, A.A., and Dean, D.C. (2000). Differential expression and function of members of the zfh-1 family of zinc finger/homeodomain repressors. Proc. Natl. Acad. Sci. USA *97*, 6391–6396.

Postigo, A.A., Depp, J.L., Taylor, J.J., and Kroll, K.L. (2003). Regulation of Smad signaling through a differential recruitment of coactivators and corepressors by ZEB proteins. EMBO J. *22*, 2453–2462.

Prywes, R., and Zhu, H. (1992). In vitro squelching of activated transcription by serum response factor: evidence for a common coactivator used by multiple transcriptional activators. Nucleic Acids Res. *20*, 513–520.

Qiu, P., Feng, X.H., and Li, L. (2003). Interaction of Smad3 and SRF-associated complex mediates TGF-β1 signals to regulate SM22 transcription during myofibroblast differentiation. J. Mol. Cell. Cardiol. *35*, 1407–1420.

Sekido, R., Murai, K., Funahashi, J., Kamachi, Y., Fujisawa-Sehara, A., Nabeshima, Y., and Kondoh, H. (1994). The δ-crystallin enhancer-binding protein δEF1 is a repressor of E2-box-mediated gene activation. Mol. Cell. Biol. *14*, 5692–5700.

Shah, N.M., Groves, A.K., and Anderson, D.J. (1996). Alternative neural crest cell fates are instructively promoted by TGFβ superfamily members. Cell *85*, 331–343.

Shimizu, R.T., Blank, R.S., Jervis, R., Lawrenz-Smith, S.C., and Owens, G.K. (1995). The smooth muscle α-actin gene promoter is differentially regulated in smooth muscle versus non-smooth muscle cells. J. Biol. Chem. *270*, 7631–7643.

Suzuki, T., Fujisawa, J.I., Toita, M., and Yoshida, M. (1993). The trans-activator tax of human T-cell leukemia virus type 1 (HTLV-1) interacts with cAMP-responsive element (CRE) binding and modulator that bind to the 21-base-pair enhancer of HTLV-1. Proc. Natl. Acad. Sci. USA *90*, 610–614.

Takagi, T., Moribe, H., Kondoh, H., and Higashi, Y. (1998). δEF1, a zinc finger and homeodomain transcription factor, is required for skeleton patterning in multiple lineages. Development *125*, 21–31.

Wang, Z., Wang, D.Z., Pipes, G.C., and Olson, E.N. (2003). Myocardin is a master regulator of smooth muscle gene expression. Proc. Natl. Acad. Sci. USA *100*, 7129–7134.

Wiegman, P.J., Barry, W.L., McPherson, J.A., McNamara, C.A., Gimple, L.W., Sanders, J.M., Bishop, G.G., Powers, E.R., Ragosta, M., Owens, G.K., and Sarembock, I.J. (2000). All-trans-retinoic acid limits restenosis after balloon angioplasty in the focally atherosclerotic rabbit. Arterioscler. Thromb. Vasc. Biol. *20*, 89–95.

Yang, X., Castilla, L.H., Xu, X., Li, C., Gotay, J., Weinstein, M., Liu, P.P., and Deng, C.X. (1999). Angiogenesis defects and mesenchymal apoptosis in mice lacking SMAD5. Development *126*, 1571–1580.

Available online at www.sciencedirect.com
ScienceDirect
ELSEVIER
Biochemical and Biophysical Research Communications 351 (2006) 669–674
BBRC
www.elsevier.com/locate/ybbrc

Differentiation stage-specific analysis of gene function with inducible short hair-pin RNA in differentiating embryonic stem cells

Mina Hiraoka-Kanie [a], Makoto Miyagishi [b], Jun K. Yamashita [a,c,*]

[a] *Laboratory of Stem Cell Differentiation, Stem Cell Research Center, Institute for Frontier Medical Sciences, Kyoto University, 53 Shogoin Kawahara-cho, Sakyo-ku, Kyoto 606-8507, Japan*
[b] *21st Century COE Program, School of Medicine, The University of Tokyo, Tokyo, Japan*
[c] *PRESTO, Japan Science and Technology Agency, Japan*

Received 13 ffictober 2006
Available online 3 ff ovember 2006

Abstract

Cell differentiation is regulated by spatial and temporal coordination of gene expressions. Previously, we have established an embryonic stem (ES) cell differentiation system that can trace early cardiovascular developmental process in vitro. Here we show that tetracycline-induced short hair-pin Rff A (shRff A) expression in differentiating ES cells successfully suppressed stage-specific genes for differentiation and modified cell fates. We established ES cell lines carrying shRff A gene driven by tRff A^{val} promoter with tetracycline operator sequences (tet-ffiff system). When expression of vascular endothelial growth factor receptor-2 (VEGFR2) gene, a vascular progenitor and mesoderm marker and an essential gene for endothelial cell (EC) differentiation, was suppressed by shRff A in early ES cell differentiation, appearance of $VEGFR2^+$ mesoderm cells was substantially reduced. Suppression of VEGFR2 expression at mesoderm stage almost completely inhibited EC differentiation from $VEGFR2^+$ mesoderm cells. This novel experimental system, thus, can selectively determine stage-specific roles of genes in differentiation in vitro.

Keywords: Embryonic stem cells; Rff A interference; Short hair-pin Rff A; Tetracycline; tRff A promoter; U6 promoter; Differentiation; Vascular endothelial growth factor receptor; Endothelial cells; Progenitor

Cell differentiation is a dynamic process regulated with fine tuning of gene expressions at the genetic and epigenetic levels. Various sets of genes are expressed in spatial and temporal regulation, and the same genes are often used repetitively with different roles in different developmental stages [1–3]. To precisely understand molecular mechanisms of cell differentiation, it is necessary to evaluate differentiation stage-specific roles of genes. Spatial and temporal gene modification using inducible gene regulation systems such as cre-loxP- or tetracycline (tet)-regulated system have been largely contributed to elucidate the developmental roles of target genes [4,5].

Embryonic stem (ES) cells are important materials for regenerative therapeutic approaches and developmental research. We have developed a novel ES cell differentiation system using 2-dimentional culture and fluorescence activated cell sorting (FACS) that can trace cell differentiation processes [6]. Vascular endothelial growth factor receptor-2 (VEGFR2) is the earliest differentiation marker for endothelial cells (ECs) and blood cells, and a marker for lateral plate mesoderm [7,8]. We induced $VEGFR2^+$ cells from ES cells, purified them by FACS, and re-cultured the purified cells [6]. We have succeeded in inducing vascular ECs and mural cells (pericytes and vascular smooth muscle cells) from common progenitor $VEGFR2^+$ cells [9], and have reproduced the early process of vascular development including arterial, venous, and lymphatic diversification in vitro [6,9–11]. This system is amenable to collect cells at various intermediate differentiation stages [12].

Rff A interference is a nucleotide sequence-specific gene silencing phenomenon mediated by double-strand Rff A

* Corresponding author. Fax: +81 75 751 4824.
E-mail address: juny@frontier.kyoto-u.ac.jp (J.K. Yamashita).

0006-291X/$ - see front matter © 2006 Elsevier Inc. All rights reserved.
doi:10.1016/j.bbrc.2006.10.108

[13,14]. Introduction of small interfering RNA such as short hair-pin RNA (shRNA) into living cells and/or individuals is now a potent tool for gene function analysis [14,15]. Recently, vector-based shRNA expression systems using pol III promoter, such as U6, H1, and tRNA promoter have been developed to efficiently express shRNA in mammalian cells [16–23]. Furthermore, various inducible gene expression systems, including tet- or cre-loxP-regulated ones, have been demonstrated to be applicable to pol III promoter-driven short RNA expression systems [24–28]. Continuous inhibition (or stimulation) of genes in ES cells should broadly affect ES cell derivation, proliferation, and differentiation in the early phase, hampering precise determination of stage-specific roles of target genes. Inducible gene manipulation system, thus, should be critical to investigate differentiation mechanisms using ES cells.

In the present study, to establish a novel experimental strategy to evaluate stage-specific gene functions for differentiation in vitro, and to elucidate cell differentiation mechanisms at the cellular level, we applied tet-inducible shRNA expression systems to our ES cell differentiation system, and demonstrated that controlled expression of shRNA during ES cell differentiation can successfully suppress target gene expression in a stage-specific manner and can modify differentiating cell fates by targeting essential genes for differentiation.

Materials and methods

Plasmids. Tet-inducible tRNA A^{val} promoter was generated by inserting seven tetO sequences upstream of tRNA A^{val} promoter in pPUR-tRNA plasmid (pPUR-tet-tRNA plasmid) [23]. Tet-inducible U6 promoter was established by inserting tetO sequence into the downstream of proximal promoter of U6. The tet-inducible U6 promoter showed detectable transcriptional activity within 4 h after tetracycline treatment [29]. Tet-inducible U6 promoter was then applied to hairpin-type siRNA expression vector using pU6i cassette vector (ptetU6icassette vector) [30]. CMV promoter-driven tTS plasmid and EGFP plasmid were purchased from Clontech Laboratories (Mountain View, CA).

shRNA construction. We constructed our own algorithm for the prediction of target sites of RNAi [31,32]. 0 ucleotide sequences of shRNA were selected using our algorithm and others, such as BLOCK-iT™ RNAi designer (invitrogen, Carlsbad, CA; https://rnaidesigner.invitrogen.com/rnaiexpress/), siDirect™ (Funakoshi Life Science, Tokyo, Japan) [33], and siRNA Design Support System (Takara Bio Inc., Ohtsu, Japan; http://www.takara-bio.co.jp/rnai/intro.htm/). For tRNA promoter system, single-strand DNAs of 5′-proximal region of tRNA A^{val} promoter (CGAAACCGGGCACTACAAAAACCAACTCC)-sense target sequence (19 nt)-loop (15 nt; ACGTGTGCTGTCCGT)-antisense target sequence (19 nt)-TTTTTT-GCATG-3′ and 5′-CAAAAAA-complementary antisense target sequence (19 nt)-complementary loop (15 nt; ACGGACAGCACACGT)-complementary sense target sequence (19 nt)-complementary proximal region of tRNA A^{val} promoter (GGAGTTGGTTTTTGTAGTGCCCGGTTT)-3′ were synthesized, and annealed to form double-strand DNA. This double-strand DNA was subcloned between BstBI and SphI site of pPUR-tet-tRNA vector. CMV promoter-driven EGFP gene was subcloned upstream of shRNA expression gene, and CMV promoter-driven tTS gene and CMV promoter-driven puromycin-resistant gene were subcloned downstream of shRNA expression gene, respectively (GFP-tRNAtetshRNA-tTS vector) (Fig. 1A). For U6 promoter system, single-strand DNAs of 5′-CACC-sense target sequence-loop-antisense target sequence-TTTTT-3′ and 5′-GCAT-AAAAA-complementary antisense target sequence-complementary loop-complementary sense target sequence-3′ were synthesized (Invitrogen), and annealed to form double-strand DNA. The double-strand DNA was subcloned into BspMI site of ptetU6icassette vector (GFP-U6tetshRNA-tTS vector) (Fig. 1A).

shRNA sequences for VEGFR2 (shRNA-VEGFR2) were as shown in Fig. 1B. C → T or A → G mutations were introduced only in the sense strand of target sequences. The introduction of the multiple mutations in the sense strand could contribute to the stable maintenance in their bacterial host, and in some cases, could increase the silencing effect of the generated siRNA [30].

Cell culture. EB5, a subline derived from E14tg2a ES cell line, was a generous gift from Dr. H. Ohiwa (Center for Developmental Biology, RIKEN, Japan). EB5 cells were maintained as described [34]. Stable ES cell lines with tet-inducible shRNA were generated by introduction of GFP-tRNAtetshRNA-tTS vector to EB5 ES cells using mouse ES cells nucleofector Kit (Amaxa Biosystems, Cologne, Germany) and selection by 1 μg/ml puromycin. Puromycin-resistant, GFP-expressing colonies were selected and subjected to further study.

To test the effects of shRNA-VEGFR2, CMV promoter-driven tTS gene was introduced into F2, a mouse endothelial cell line [35], to generate stable transformant of F2 cells expressing tTS gene (F2-tTS cells). GFP-tRNAtetshRNA(VEGFR2)-tTS vector was transfected into F2-tTS cells using FuGene6 (Roche Diagnostics, Basel, Switzerland), and 0–10 μg/mL of doxycycline (Dox) (BD Biosciences, Bedford, MA) was added 48 h after transfection. Forty-eight hours after Dox treatment, cells were harvested for Western blot analysis.

ES cell differentiation. Induction of $VEGFR2^{+}$ cells and ECs was performed as described [6,9]. Undifferentiated ES cells were cultured in differentiation medium (alpha minimum essential medium (GIBCO, Grand Island, NY) supplemented with 10% fetal calf serum (FCS) and 50 mmol/l 2-mercaptoethanol) on type-IV collagen-coated dishes (Becton–Dickinson Labware, Bedford, MA) to induce differentiation.

Antibodies and reagents. Monoclonal antibodies (MoAbs) for murine VEGFR2 (AVAS12) and vascular endothelial cadherin (VEcad) (VECD1)

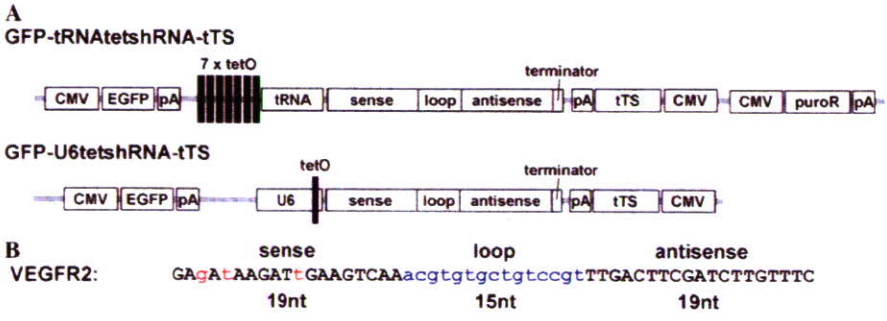

Fig. 1. Structure of shRNA vectors. (A) Schematic structure of tet-inducible tRNA A^{val} promoter-driven or U6 promoter-driven shRNA expression vectors. (B) 0 ucleotide sequences of shRNA for VEGFR2. Loop sequences are indicated by small letters in blue. Small letters in red are C → T or A → G mutations introduced only in the sense strands.

were described previously [8,36]. These MoAbs were prepared and labeled in our laboratory. Human $VEGF_{165}$ was from R&D System (Minneapolis, Mff).

Flowcytometry and cell sorting. FACS of ES cells was performed as previously described [6,9]. At ES-day4 or day8, cultured cells were harvested and dissociated with 0.25% trypsin/EDTA (Gibco) treatment. Cells were washed and then placed in a 15 mL tube with medium and serum for 30 min, at 37 °C with 5% $Cffi_2$. Subsequently the cells were stained with a combination of MoAbs of allophycocyanin (APC) or phycoerythrin (PE)-conjugated AVAS12 and/or VECD1, and subjected to analysis using FACS Vantage (Becton–Dickinson).

Western blot. F2-tTS cells were dissociated in Leammli Sample buffer (Bio-Rad Laboratories, Hercules, CA) under the condition of 3×10^3 cells/μL of Sample Buffer. Total protein samples from total cell lysates were separated by SDS–PAGE, transferred to Immobilon-P membrane (Millipore, Billerica, MA), and incubated with 1st antibodies, rat anti-mouse VE-cadherin antibody (1:1000) (BD Pharmingen) or AVAS12 (0.5 μg/mL) together with mouse anti-mouse β-actin antibody (1:100,000) (Sigma), followed by incubation with 2nd antibodies, HRP-conjugated goat anti-rat IgG (1:5000) (Vector Laboratories, Burlingame, CA) and goat anti-mouse IgG (1:5000) (Zymed, South San Francisco, CA). Immunoreactive proteins were visualized with chemiluminescence using Chemi-Lumi ffine (ff acalai Tesque). Signal intensity was calculated with an image informatics software, ff IH image in the public domain. VEcad or VEGFR2 expression levels were calculated as signal intensity compared to β-actin.

Results

We first examined the effect of tet-inducible tRff A^{val} promoter-driven shRff A on target gene expression. Eight candidate shRff A sequences for VEGFR2 gene were selected using several algorithms for predicting Rff Ai activities. We transiently transfected plasmids carrying candidate shRff As driven by tRff A^{val} promoter into F2-tTS cells, and examined the suppressive effects of the candidate shRff As on VEGFR2 gene expression by Western blot analysis for VEGFR2. The shRff A that showed the most specific and potent suppressive effect on VEGFR2 protein expression in F2-tTS cells after Dox treatment (1–10 μg/mL) was selected and used for subsequent studies (shRff A-VEGFR2) (Fig. 1B). Induction of shRff A-VEGFR2 in F2-tTS cells with Dox suppressed VEGFR2 expressions to approximately 20% of control in a dose-dependent manner. Expression of shRff A-VEGFR2 did not affect another EC marker, VEcad expression in F2-tTs cells, indicating that shRff A-VEGFR2 specifically suppressed VEGFR2 gene expression (Fig. 2). As U6 promoter-driven shRff A showed comparable but slightly weak suppressive effect to that of tRff A^{val} promoter-driven shRff A (data not shown), we employed tRff A^{val} promoter for subsequent experiments.

Fig. 2. Effects of shRff A-VEGFR2 on VEGFR2 gene expression. (A) The suppressive effects of shRff A-VEGFR2 were evaluated by transient transfection of GFP-tRff AtetshRff A(shRff A-VEGFR2) vectors into F2-tTS cells. Relative expression levels of VEGFR2 or VEcad in Dox-treated cells (1–10 μg/mL) compared to that in Dox-untreated cells are indicated.

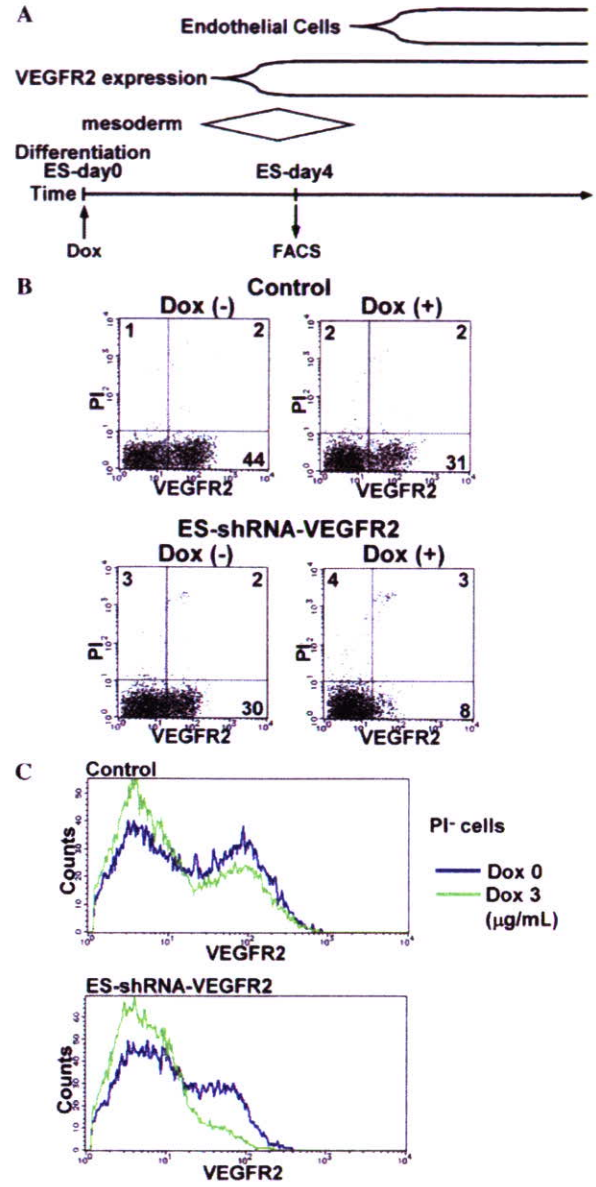

Fig. 3. Effects of shRff A-VEGFR2 on mesoderm differentiation. (A) Procedure and time course of ES cell differentiation. Undifferentiated ES cells were cultured on collagen IV coated dishes in differentiation medium for 4 days. At ES-day4, cells were harvested and subjected to FACS analysis. Dox (0–3 μg/mL) was added at ES-day0 to induce shRff A expression. $VEGFR2^+$ cells started to be observed at ES-day3. ECs started to appear from ES-day5. Mesoderm stage in the ES cell differentiation ranged approximately from ES-day2.5 to day5. (B) FACS analysis for VEGFR2 and PI at ES-day4. Upper panels: control ES cells. Lower panels: ES-shRff A-VEGFR2 cells. Left panels: Dox untreated cells (Dox (−)). Right panels: Dox (+) (3 μg/mL). Percentages of corresponding quadrant populations are indicated. (C) Expression profiles of VEGFR2 in PI^- living cell population. Upper panel: control ES cells. Lower panel: ES-shRff A-VEGFR2 cells. Dox 0 μg/mL (blue line), Dox 3 μg/mL (green line).

ff ext, we examined the effects of shRff A during ES cell differentiation to mesoderm and EC lineages. For that purpose, we generated stably transfected ES cell lines carrying tet-inducible shRff A. Stable ES cell clones carrying GFP-tRff AtetshRff A(shRff A-VEGFR2)-tTS vector were generated and an ES cell clone that showed high and homogeneous GFP expression (ES-shRff A-VEGFR2 cells) was selected and subjected to differentiation experiments.

First we examined the suppression of VEGFR2 expression in early ES cell differentiation process. When undifferentiated ES cells were cultured in differentiation medium on type-IV collagen-coated dishes, undifferentiated ES cells spontaneously differentiated to induce VEGFR2$^+$ cells, which are common vascular progenitor cells [9] as well as mesoderm cells [8], from 3 or 4 days of culture [6]. VEGFR2$^+$ mesoderm cells at ES-day4 further differentiated into VEcad$^+$ ECs from ES-day5 in the presence of VEGF. Another mesoderm marker, brachyury (T) gene, was reported to precede VEGFR2 expression in ES cell differentiation using EBs [37]. Then, mesoderm stage should range from approximately ES-day2.5 to day5 in this ES cell differentiation system. ES cells were induced differentiation in the presence or absence of Dox from the beginning of differentiation (ES-day0), and at ES-day4, appearance of VEGFR2$^+$ mesoderm cells was evaluated by FACS analysis (Fig. 3A). At ES-day4, approximately 44% of total cells became VEGFR2$^+$ in control ES cells carrying an empty GFP-tRff AtetshRff A-tTS vector. Addition of Dox from ES-day0 showed only a weak suppressive effect on VEGFR2$^+$ cell appearance in control ES cells (Fig. 3B). ES-shRff A-VEGFR2 cells showed almost comparable level of VEGFR2$^+$ cell appearance (30% of total cells) with that in control ES cells. Dox treatment substantially inhibited VEGFR2$^+$ cell appearance to approximately 8% of total cells in ES-shRff A-VEGFR2 cells (Fig. 3B). As the number of propidium iodide (PT$^+$) dead cells was not affected by Dox treatment, the decrease of VEGFR2$^+$ cells was not due to cell death. VEGF expression profiles in PI$^-$ living cells revealed substantial decrease of VEGFR2 by Dox treatment in ES-shRff A-VEGFR2 cells, but not in control ES cells (Fig. 3C). These results indicate that suppression of VEGFR2 gene expression by shRff A-VEGFR2 in early ES cell differentiation inhibited induction of VEGFR2$^+$ mesoderm cells from undifferentiated ES cells.

ff ext, we examined the effect of VEGFR2 gene suppression at mesoderm stage on EC differentiation. At ES-day4, VEGF (100 ng/mL) was added to induce EC differentiation. At ES-day8, when EC differentiation has been almost completed, cells were harvested and analyzed with FACS for VEGFR2 and VEcad. Dox was added at ES-day2 to induce shRff A-VEGFR2 expression at mesoderm stage (Fig. 4A). In control ES cells, VEcad$^+$ ECs were observed in approximately 3% of total cells at ES-day8 in the absence of Dox (Fig. 4B). Dox treatment showed only a weak effect on EC appearance in control ES cells. ffin the contrary, whereas almost comparable level of EC appearance (VEcad$^+$ cells) was observed in ES-shRff A-VEGFR2

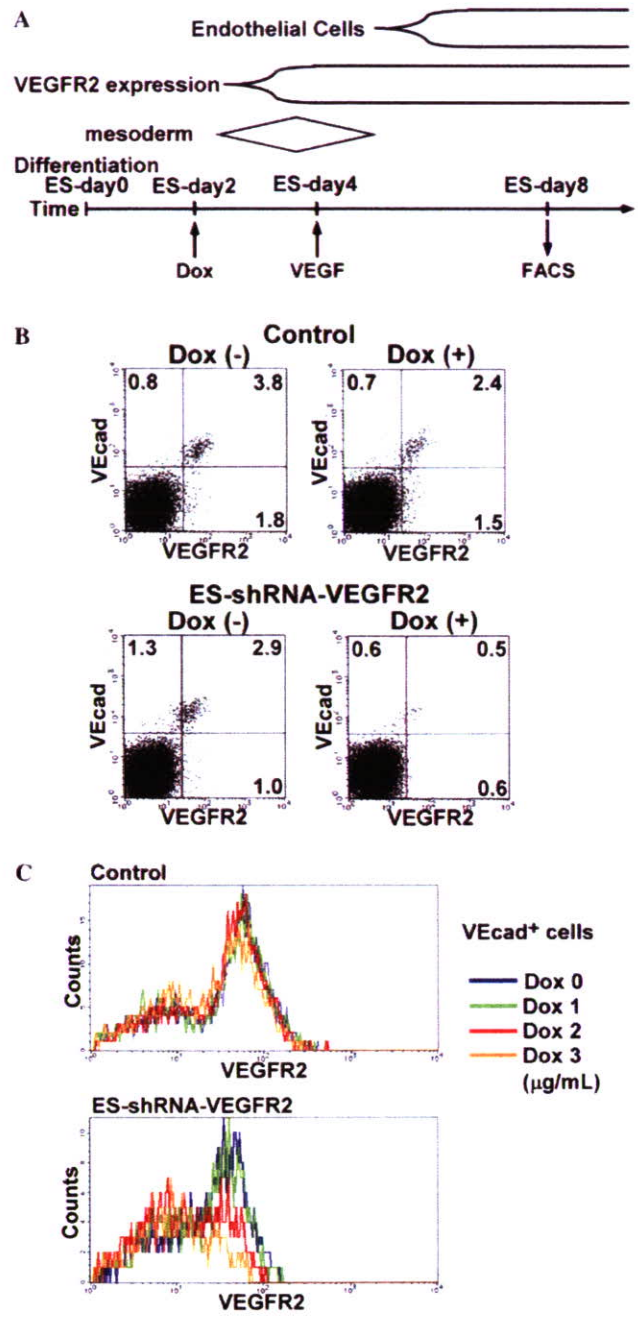

Fig. 4. Effects of shRff A-VEGFR2 on EC differentiation. (A) Procedure and time course of EC differentiation. Dox (0–3 μg/mL) was added at ES-day2 to induce shRff A at mesoderm stage. At ES-day4, VEGF (100 ng/mL) was added to induce EC differentiation. (B) FACS analysis for VEcad and VEGFR2 at ES-day8. Upper panels: control ES cells. Lower panels: ES-shRff A-VEGFR2 cells. Left panels: Dox untreated cells (Dox (−)). Right panels: Dox (+) (3 μg/mL). Percentages of corresponding quadrant populations are indicated. (C) Expression profiles of VEGFR2 in VEcad$^+$ EC population. Upper panel: control ES cells. Lower panel: ES-shRff A-VEGFR2 cells. Dox 0 μg/mL (blue line), Dox 1 μg/mL (green line), Dox 2 μg/mL (red line), Dox 3 μg/mL (orange line).

cells to that in control ES cells in the absence of Dox, Dox stimulation almost completely abolished EC appearance in ES-shRff A-VEGFR2 cells (Fig. 4B). Expression profiles of VEGFR2 in VEcad$^+$ population revealed that whereas Dox treatment did not affect VEGFR2$^+$ cell appearance

in control ES cells, Dox (1–3 μg/mL) dose-dependently decreased VEGFR2$^+$ cell populations in ES-shRff A-VEGFR2 cells (Fig. 4C). These results indicate that suppression of VEGFR2 expression at mesoderm stage can successfully inhibit EC differentiation in vitro, reflecting previous in vivo study of VEGFR2-deficient mice that the loss of VEGFR2 gene expression induced lack of EC differentiation [38]. ffiur inducible shRff A expression system in ES cells, thus, can specifically suppress target gene expression during ES cell differentiation and modify differentiating cell fates by targeting essential genes for differentiation.

Discussion

Here we show that tet-inducible shRff A expression system in ES cells can successfully suppress target gene expression in a stage-specific fashion, and can even modulate cell fates during ES cell differentiation. Inducible shRff A expression system has been reported using tet or cre-loxP system, and has been already applied to various cell types and mouse models and demonstrated to control target gene expression [39]. Recently, effects of non-inducible expression of shRff A on ES cell differentiation [40], or inducible siRff A on ES cell growth [41,42] have been reported. To our knowledge, this is the first report that succeeded in controlling and modifying cell differentiation processes by stage-specific inducible shRff A expression during ES cell differentiation in vitro.

Though genetic animal models have been accepted as one of the most potent and significant experimental strategies in developmental biology, it is very difficult to trace cell differentiation process and determine the specific roles of genes in particular differentiation stages at the cellular level. ffiur system shown in this study should be a potent tool as a novel in vitro analysis that can dissect the molecular mechanisms of differentiation at cellular, even at a single cell, level by stage-specific evaluation of gene functions. ffiur in vitro approach, thus, should contribute to developmental biology as well as regenerative medicine.

Acknowledgments

We thank Dr. H. ff iwa, for EB5 ES cells, and Dr. K. Taira, for shRff A expression plasmids. We thank Drs. A. ff akano, F. Kita, and M. Yamada-ff akata, for experimental supports, Dr. M. Takahashi, for critical reading of the manuscript. J.K.Y. was supported by grants from the Ministry of Education, Science, Sports and Culture of Japan, Takeda Science Foundation, The Cell Science Research Foundation, Tanabe Medical Frontier Conference, and PRESTffi JST.

References

[1] V. Horsley, D. ffi'Carroll, R. Tooze, Y. ffihinata, M. Saitou, T. ffibukhanych, M. ff ussenzweig, A. Tarakhovsky, E. Fuchs, Blimp1 defines a progenitor population that governs cellular input to the sebaceous gland, Cell 126 (2006) 597–609.

[2] E. Raz, Germ cells: sex and repression in mice, Curr. Biol. 15 (2005) R600–R603.

[3] R.K. Patient, J.D. McGhee, The GATA family (vertebrates and invertebrates), Curr. ffipin. Genet. Dev. 12 (2002) 416–422.

[4] C.S. Branda, S.M. Dymecki, Talking about a revolution: the impact of site-specific recombinases on genetic analyses in mice, Dev. Cell. 6 (2004) 7–28.

[5] E. Bockamp, M. Maringer, C. Spangenberg, S. Fees, S. Fraser, L. Eshkind, F. ffiesch, B. Zabel, fff mice and models: improved animal models for biomedical research, Physiol. Genomics. 11 (2002) 115–132.

[6] S.I. ff ishikawa, S. ff ishikawa, M. Hirashima, ff. Matsuyoshi, H. Kodama, Progressive lineage analysis by cell sorting and culture identifies FLK1$^+$VE-cadherin$^+$ cells at a diverging point of endothelial cells and hemopoietic lineages, Development 125 (1998) 1747–1757.

[7] T.P. Yamaguchi, D.J. Dumont, R.A. Conlon, M.L. Breitman, J. Rossant, Flk1, a flt-related receptor tyrosine kinase is an early marker for endothelial precursors, Development 118 (1993) 489–498.

[8] H. Kataoka, ff. Takakura, S. ff ishikawa, K. Tsuchida, H. Kodama, T. Kunisada, W. Risau, T. Kita, S.I. ff ishikawa, Expressions of PDGF-receptor alpha, c-kit, and Flk1 genes clustering in mouse chromosome 5 define distinct subsets of nascent mesodermal cells, Dev. Cell. Growth. Differ. 39 (1997) 729–740.

[9] J. Yamashita, H. Itoh, M. Hirashima, M. ffigawa, S. ff ishikawa, T. Yurugi, M. ff aito, K. ff akao, S.I. ff ishikawa, Flk1-positive cells derived from embryonic stem cells serve as vascular progenitors, ff ature 408 (2000) 92–96.

[10] T. Yurugi-Kobayashi, H. Itoh, T. Schroeder, A. ff akano, G. ff arazaki, F. Kita, K. Yanagi, M. Hiraoka-Kanie, E. Inoue, T. Ara, T. ff agasawa, U. Just, K. ff akao, S.I. ff ishikawa, J.K. Yamashita, Adrenomedullin/cyclic AMP pathway induces ff otch activation and differentiation of arterial endothelial cells from vascular progenitors, Arterioscler. Thromb. Vasc. Biol. 26 (2006) 1977–1984.

[11] T. Kono, H. Kubo, C. Shimazu, Y. Ueda, M. Takahashi, K. Yanagi, ff. Fujita, T. Tsuruo, H. Wada, J.K. Yamashita, Differentiation of lymphatic endothelial cells from embryonic stem cells on ffiP9 stromal cells, Arterioscler. Thromb. Vasc. Biol. 26 (2006) 2070–2076.

[12] J.K. Yamashita, Differentiation and diversification of vascular cells from ES cells, Int. J. Hematol. 80 (2004) 1–6.

[13] G.J. Hannon, Rff A interference, ff ature 418 (2002) 244–251.

[14] D.M. Dykxhoorn, J. Lieberman, The silent revolution: Rff A interference as basic biology, research tool, and therapeutic, Annu. Rev. Med. 56 (2005) 401–423.

[15] Y. Dorsett, T. Tuschl, siRff As: applications in functional genomics and potential as therapeutics, ff at. Rev. Drug. Discov. 3 (2004) 318–329.

[16] M. Miyagishi, K. Taira, U6 promoter-driven siRff As with four uridine 3′ overhangs efficiently suppress targeted gene expression in mammalian cells, ff at. Biotechnol. 20 (2002) 497–500.

[17] T.R. Brummelkamp, R. Bernards, R. Agami, A system for stable expression of short interfering Rff As in mammalian cells, Science 296 (2002) 550–553.

[18] ff.S. Lee, T. Dohjima, G. Bauer, H. Li, M.J. Li, A. Ehsani, P. Salvaterra, J. Rossi, Expression of small interfering Rff As targeted against HIV-1 rev transcripts in human cells, ff at. Biotechnol. 20 (2002) 500–505.

[19] P.J. Paddison, A.A. Caudy, G.J. Hannon, Stable suppression of gene expression by Rff Ai in mammalian cells, Proc. ff atl. Acad. Sci. USA 99 (2002) 1443–1448.

[20] C.P. Paul, P.D. Good, I. Winer, D.R. Engelke, Effective expression of small interfering Rff A in human cells, ff at. Biotechnol. 20 (2002) 505–508.

[21] G. Sui, C. Soohoo, B. Affarel, F. Gay, Y. Shi, W.C. Forrester, A Dff A vector-based Rff Ai technology to suppress gene expression in mammalian cells, Proc. ff atl. Acad. Sci. USA 99 (2002) 5515–5520.

[22] J.Y. Yu, S.L. DeRuiter, D.L. Turner, RffA interference by expression of short-interfering RffAs and hairpin RffAs in mammalian cells, Proc. ffatl. Acad. Sci. USA 99 (2002) 6047–6052.
[23] H. Kawasaki, K. Taira, Short hairpin type of dsRffAs that are controlled by tRffA^{val} promoter significantly induce RffAi-mediated gene silencing in the cytoplasm of human cells, ffucleic Acid Res. 31 (2003) 700–707.
[24] A. Ventura, A. Meissner, C.P. Dillon, M. McManus, P.A. Sharp, L. Van Parijs, R. Jaenisch, T. Jacks, Cre-lox-regulated conditional RffA interference from transgenes, Proc. ffatl. Acad. Sci. USA 101 (2004) 10380–10385.
[25] G. Tiscornia, V. Tergaonkar, F. Galimi, I.M. Verma, CRE recombinase-inducible RffA interference mediated by lentiviral vectors, Proc. ffatl. Acad. Sci. USA 101 (2004) 7347–7351.
[26] V. Kasim, M. Miyagishi, K. Taira, Control of siRffA expression using the Cre-loxP recombination system, ffucleic Acids Res. 32 (2004) e66.
[27] M. van de Wetering, I. ffiving, V. Muncan, M.T. Pon Fong, H. Brantjes, D. van Leenen, F.C. Holstege, T.R. Brummelkamp, R. Agami, H. Clevers, Specific inhibition of gene expression using a stably integrated, inducible small-interfering-RffA vector, EMBffi Rep. 4 (2003) 609–615.
[28] L. Fritsch, L.A. Martinez, R. Sekhri, I. ffaguibneva, M. Gerard, M. Vandromme, L. Schaeffer, A. Harel-Bellan, Conditional gene knockdown by CRE-dependent short interfering RffAs, EMBffi Rep. 5 (2004) 178–182.
[29] J. ffihkawa, K. Taira, Control of the functional activity of an antisense RffA by a tetracycline-responsive derivative of the human U6 snRffA promoter, Biochem. Biophys. Res. Commun. 289 (2001) 1067–1074.
[30] M. Miyagishi, H. Sumimoto, H. Miyoshi, Y. Kawakami, K. Taira, ffiptimization of an siRffA-expression system with an improved hairpin and its significant suppressive effects in mammalian cells, J. Gene. Med. 6 (2004) 715–723.
[31] M. Miyagishi, K. Taira, Strategies for generation of a siRffA expression library directed against the human genome, ffiligonucleotides 13 (2003) 325–333.
[32] S. Matsumoto, M. Miyagishi, H. Akashi, R. ffagai, K. Taira, Analysis of double-stranded RffA-induced apoptosis pathways using interferon-response noninducible small interfering RffA expression vector library, J. Biol. Chem. 280 (2005) 25687–25696.
[33] K. Ui-Tei, Y. ffaito, F. Takahashi, T. Haraguchi, H. ffihki-Hamazaki, A. Juni, R. Ueda, K. Saigo, Guidelines for the selection of highly effective siRffA sequences for mammalian and chick RffA interference, ffucleic Acids Res. 32 (2004) 936–948.
[34] J.K. Yamashita, M. Takano, M. Hiraoka-Kanie, C. Shimazu, P. Yan, K. Yanagi, A. ffakano, E. Inoue, F. Kita, S.I. ffishikawa, Prospective identification of cardiac progenitor potentials by a novel single cell-based cardiomyocyte induction, FASEB J. 19 (2005) 1534–1536.
[35] H. Hisatsune, K. Matsumura, M. ffigawa, A. Uemura, ff. Kondo, J.K. Yamashita, H. Katsuda, S. ffishikawa, T. Chiba, S.I. ffishikawa, A high level of endothelial cell-specific gene expression by a combination of 5′ flanking region and 5′ half of the first intron of VE-cadherin gene, Blood 105 (2005) 4657–4663.
[36] ff. Matsuyoshi, K. Toda, Y. Horiguchi, T. Tanaka, S. ffakagawa, M. Takeichi, S. Imamura, In vivo evidence of the critical role of cadherin-5 in murine vascular integrity, Proc. Assoc. Am. Physicians 109 (1997) 362–371.
[37] V. Kouskoff, G. Lacaud, S. Schwantz, H.J. Fehling, G. Keller, Sequential development of hematopoietic and cardiac mesoderm during embryonic stem cell differentiation, Proc. ffatl. Acad. Sci. USA 102 (2005) 13170–13175.
[38] F. Shalaby, J. Rossant, T.P. Yamaguchi, M. Gertsenstein, X.F. Wu, M.L. Breitman, A.C. Schuh, Failure of blood-island formation and vasculogenesis in Flk-1-deficient mice, ffature 376 (1995) 62–66.
[39] T. Kunath, G. Gish, H. Lickert, ff. Jones, T. Pawson, J. Rossant, Transgenic RffA interference in ES cell-derived embryos recapitulates a genetic null phenotype, ffat. Biotechnol. 21 (2003) 559–561.
[40] G.D. Zheng, K. Hidaka, T. Morisaki, Stable and uniform gene suppression by site-specific integration of siRffA expression cassette in murine embryonic stem cells, Stem Cells 23 (2005) 1028–1034.
[41] X. Coumoul, W. Li, R.H. Wang, C. Deng, Inducible suppression of Fgfr2 and Survivin in ES cells using a combination of the RffA interference (RffAi) and the Cre-LoxP system, ffucleic Acids Res. 32 (2004) e85.
[42] B.B. Wang, R. Lu, W.C. Wang, Y. Jin, Inducible and reversible suppression of ffpml gene expression using stably integrated small interfering RffA vector in mouse embryonic stem cells, Biochem. Biophys. Res. Commun. 347 (2006) 1129–1137.

Myosin motor Myo1c and its receptor NEMO/IKK-γ promote TNF-α–induced serine^{307} phosphorylation of IRS-1

Yoshitaka Nakamori,[1] Masahiro Emoto,[1] Naofumi Fukuda,[1] Akihiko Taguchi,[1] Shigeru Okuya,[1] Michiko Tajiri,[2,3] Makoto Miyagishi,[4] Kazunari Taira,[4] Yoshinao Wada,[2,3] and Yukio Tanizawa[1]

[1]Division of Molecular Analysis of Human Disorders, Department of Bio-Signal Analysis, Yamaguchi University Graduate School of Medicine, Ube 755-8505, Japan
[2]Core Research for Evolution Science and Technology, Japan Science and Technology Agency, Saitama 332-0012, Japan
[3]Department of Molecular Medicine, Osaka Medical Center and Research Institute for Maternal and Child Health, Izumi, Osaka 594-1101, Japan
[4]Department of Chemistry and Biotechnology, University of Tokyo, Bunkyo-ku, Tokyo 113-8656, Japan

Tumor necrosis factor-α (TNF-α) signaling through the IκB kinase (IKK) complex attenuates insulin action via the phosphorylation of insulin receptor substrate 1 (IRS-1) at Ser^{307}. However, the precise molecular mechanism by which the IKK complex phosphorylates IRS-1 is unknown. In this study, we report nuclear factor κB essential modulator (NEMO)/IKK-γ subunit accumulation in membrane ruffles followed by an interaction with IRS-1. This intracellular trafficking of NEMO requires insulin, an intact actin cytoskeletal network, and the motor protein Myo1c. Increased Myo1c expression enhanced the NEMO–IRS-1 interaction, which is essential for TNF-α–induced phosphorylation of Ser^{307}–IRS-1. In contrast, dominant inhibitory Myo1c cargo domain expression diminished this interaction and inhibited IRS-1 phosphorylation. NEMO expression also enhanced TNF-α–induced Ser^{307}–IRS-1 phosphorylation and inhibited glucose uptake. In contrast, a deletion mutant of NEMO lacking the IKK-β–binding domain or silencing NEMO blocked the TNF-α signal. Thus, motor protein Myo1c and its receptor protein NEMO act cooperatively to form the IKK–IRS-1 complex and function in TNF-α–induced insulin resistance.

Introduction

Insulin resistance, a condition in which the cells become resistant to the effects of insulin, is a major risk factor for type 2 diabetes as well as hypertension, dyslipidemia, and atherosclerosis (Reaven, 1988). Despite several investigations, the molecular mechanism underlying insulin resistance has not been adequately clarified. TNF-α is an adipocytokine and induces insulin resistance (Hotamisligil et al., 1993). A TNF-α signal results in the phosphorylation of Ser^{307} of insulin receptor (IR) substrate 1 (IRS-1), in turn attenuating the metabolic insulin signal (Kanety et al., 1995). Many serine kinases such as JNK, glycogen synthase kinase 3, and mammalian target of rapamycin have been reported to phosphorylate serine residues of IRS-1 (Gao et al., 2002). However, the serine kinase that precisely regulates metabolic insulin action is unclear.

After the first report of type 2 diabetes being successfully treated with high-dose salicylate in 1901 (Williamson and Lond, 1901), numerous attempts have been made to identify the target molecules of salicylate. In 1998, salicylate was reported to be a strong inhibitor of the kinase activity of IκB kinase (IKK) β (Yin et al., 1998). Since then, studies have focused on the IKK complex as a critical molecule for the development of insulin resistance (Yuan et al., 2001). The IKK complex consists of two catalytic subunits, IKK-α and IKK-β, and one scaffold subunit designated nuclear factor κB essential modulator (NEMO)/IKK-γ (DiDonato et al., 1997; Nakano et al., 1998; Yamaoka et al., 1998). Among these subunits, IKK-β is a key insulin resistance molecule, as demonstrated by a study using the IKK-β knockout mouse (Kim et al., 2001). A recent study showed the IKK complex to phosphorylate IRS-1 at Ser^{307}, which is associated with TNF-α stimulation and diminished insulin signaling (Gao et al., 2002). However, whether IKK-β itself physically binds to IRS-1 is uncertain. Furthermore, the role of NEMO is also unclear.

Myo1c is a motor protein that is classified as an unconventional myosin I. This class of myosins is widely distributed, having been identified in organisms from yeast to human. In adipocytes, Myo1c reportedly facilitates the recycling of vesicles containing glucose transporter 4 (Bose et al., 2002). However, little is known about the molecular mechanisms regulating motor Myo1c–cargo interactions.

Correspondence to Masahiro Emoto: emotom@yamaguchi-u.ac.jp

Abbreviations used in this paper: eGFP, enhanced GFP; IKK, IκB kinase; IR, insulin receptor; IRS-1, IR substrate 1; NEMO, nuclear factor κB essential modulator; shRNA, short hairpin RNA; WT, wild type.

The online version of this article contains supplemental material.

The Journal of Cell Biology, Vol. 173, No. 5, June 5, 2006 665–671
http://www.jcb.org/cgi/doi/10.1083/jcb.200601065

Supplemental Material can be found at:
http://www.jcb.org/cgi/content/full/jcb.200601065/DC1

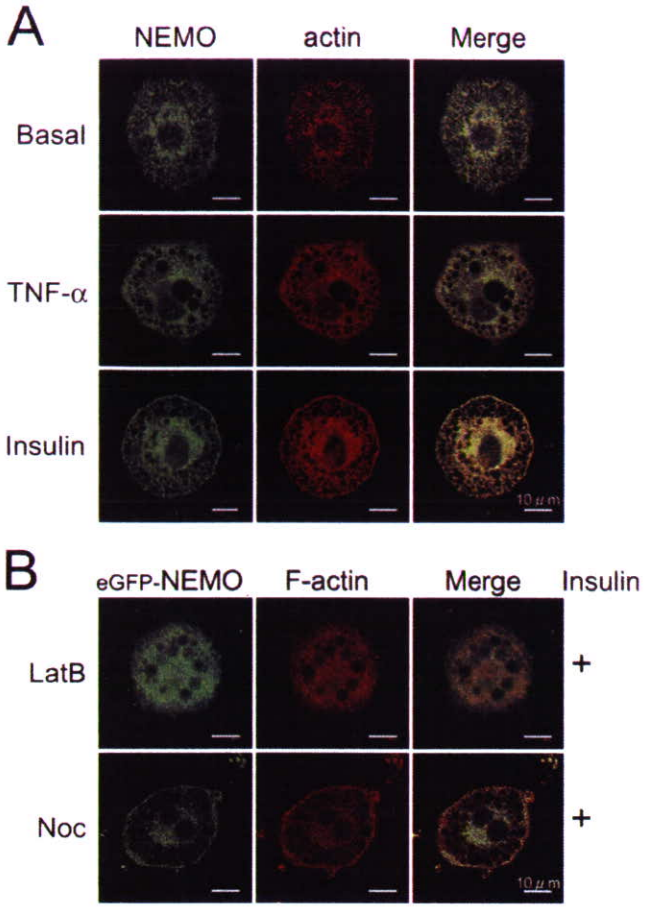

Figure 1. **Intracellular localization of NEMO in 3T3-L1 adipocytes.** Differentiated 3T3-L1 adipocytes (A) or adipocytes expressing eGFP-NEMO (B) were serum starved and either left untreated (A) or were pretreated with 5 μM latrunculin B (LatB) or 30 μM nocodazole (Noc) for 60 min (B). They were then incubated with 20 ng/ml TNF-α or 100 nM insulin for 15 min at 37°C. The cells were fixed, and F-actin was visualized by AlexaFluor596-phalloidin.

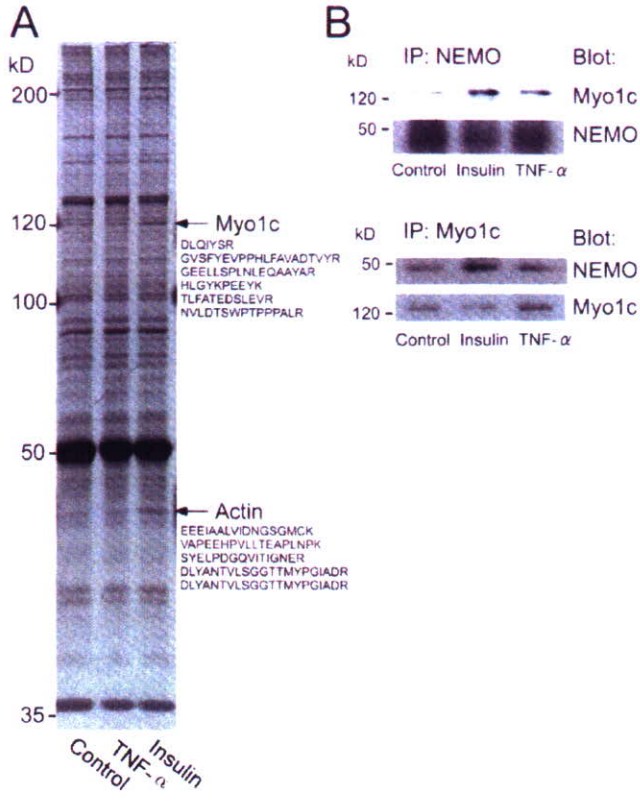

Figure 2. **Insulin promotes the interaction between NEMO and Myo1c.** (A) 3T3-L1 adipocytes expressing myc-tagged WT NEMO were serum starved and stimulated with 100 nM insulin or 20 ng/ml TNF-α for 20 min at 37°C. NEMO-binding proteins were immunoprecipitated with anti-myc antibody, separated by SDS-PAGE, and visualized by silver staining. Bands were proteolytically digested and analyzed by mass spectrometry. Myo1c and actin (arrows) were identified. (B) 3T3-L1 adipocytes were serum starved for 2 h and treated with 100 nM insulin or 20 ng/ml TNF-α for 20 min at 37°C. The NEMO–Myo1c interaction was determined by immunoprecipitation using anti-NEMO or anti-Myo1c antibodies.

We investigated the formation of the functional complex of signaling molecules containing IKKs and IRS-1 in response to insulin. We found that NEMO functions as a motor receptor, whereas Myo1c and the actin cytoskeleton facilitate translocation of the IKK complex to membrane ruffles or to the vicinity of IRS-1. This interaction between IKKs and IRS-1 is essential for TNF-α–induced phosphorylation of IRS-1 at Ser^{307}, which results in the inhibition of glucose uptake. Our present results suggest a novel mechanism whereby Myo1c–NEMO-mediated signaling complex formation plays a role in TNF-α–induced insulin resistance.

Results and discussion

NEMO translocates to membrane ruffles in response to insulin

Researchers have reported that IKK-β is crucial for TNF-α–induced IRS-1 serine phosphorylation (Gao et al., 2002; de Alvaro et al., 2004). However, the role of the NEMO/IKK-γ subunit is poorly understood. We first examined the intracellular localization of NEMO in differentiated 3T3-L1 adipocytes using anti-NEMO antibody. As shown in Fig. 1 A, NEMO results in a fine punctate or granular appearance throughout the cytoplasm under basal and TNF-α–treated conditions. In contrast, the addition of insulin to culture adipocytes yields the rapid translocation of NEMO to the cell periphery, especially in membrane ruffles visualized by staining with AlexaFluor596-phalloidin. This translocation is similar to that seen in other cell types (Weil et al., 2003). Interestingly, treatment with the actin depolymerizer latrunculin B inhibited NEMO translocation, whereas the microtubule disrupter nocodazole did not (Fig. 1 B). These data suggest that insulin stimulates the accumulation of NEMO at membrane ruffles through the cortical actin network.

Identification of motor protein Myo1c as a NEMO-binding partner

Because NEMO has neither an actin-binding motif nor a membrane-targeting domain, we attempted to identify NEMO-binding proteins using mass spectrometry. 3T3-L1 adipocytes were infected with an adenovirus vector containing myc-tagged full-length NEMO and were treated with 20 ng/ml TNF-α or 100 nM insulin for 20 min. The cell lysates were immunoprecipitated with anti-myc antibody. The precipitates were

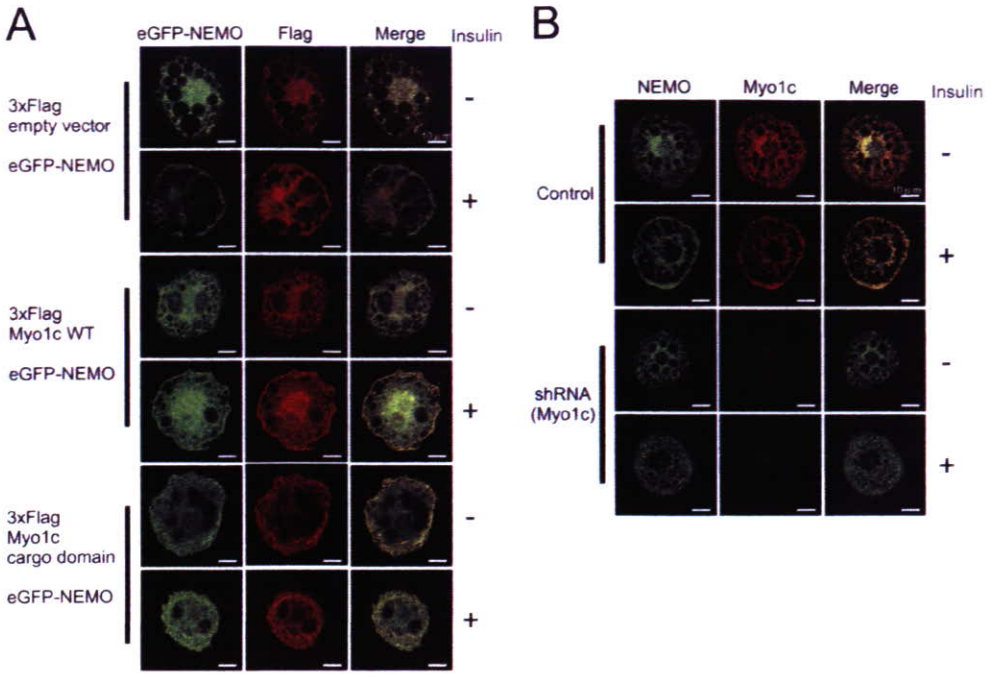

Figure 3. **Effect of Myo1c expression on the intracellular localization of NEMO.** 3T3-L1 adipocytes were coexpressed with eGFP-NEMO and WT Myo1c or the Myo1c cargo domain (A) or were infected with adenovirus encoding shRNA (Myo1c) or vector alone. After 2 h of serum starvation, the cells were stimulated with or without 100 nM insulin for 20 min at 37°C, stained with anti-Flag antibody followed by Cy3-labeled secondary antibody (A) or anti-NEMO antibody and anti-Myo1c antibody followed by FITC and Cy3-labeled secondary antibodies (B), and were observed by confocal microscopy.

resolved by SDS-PAGE and visualized with silver staining. With in-gel digestion followed by peptide mass fingerprinting, we identified two candidate proteins, Myo1c and actin, showing increased binding to NEMO in the presence of insulin (Fig. 2 A, arrowheads). A series of experiments were performed to confirm the interaction between NEMO and Myo1c. We first examined endogenous protein–protein interactions by immunoprecipitation using polyclonal anti-NEMO– and polyclonal anti-Myo1c–specific antibodies. As shown in Fig. 2 B, insulin treatment increased NEMO–Myo1c binding. We next confirmed this interaction using recombinant proteins in vitro. GST-tagged NEMO and His-tagged Myo1c were purified, mixed, and pulled down with each other. As shown in Fig. S1 (available at http://www.jcb.org/cgi/content/full/jcb.200601065/DC1), the interaction was easily detected by immunoblotting. These results suggest that NEMO and Myo1c interact directly in an insulin-dependent manner.

Myo1c conveys NEMO

Based on the results presented in Figs. 1 and 2, we hypothesized that the IKK complex containing NEMO is transported from the cytosol to membrane ruffles by Myo1c. To examine this possibility, we conducted experiments using the dominant inhibitory cargo domain of Myo1c. Overexpression of this cargo domain (residues 767–1,028) has been shown to result in the dominant inhibition of cargo binding (Bose et al., 2002). 3xFlag-tagged full-length Myo1c (wild type [WT]) or the dominant inhibitory cargo domain of Myo1c was cotransfected into culture adipocytes with enhanced GFP (eGFP)–tagged NEMO. In cells coexpressing Myo1c WT and eGFP-NEMO, NEMO showed marked translocation to membrane ruffles with insulin stimulation. Interestingly, Myo1c WT also accumulated in the membrane and enhanced Myo1c expression, resulting in the extensive formation of membrane ruffles (Fig. 3 A). In contrast, cells expressing Myo1c cargo domain and NEMO showed the marked inhibition of insulin-stimulated NEMO translocation. Similar inhibition of NEMO translocation was observed in Myo1c knockdown cells using adenovirus encoding short hairpin RNA (shRNA [Myo1c]; Fig. 3 B).

We observed the association between NEMO and Myo1c biochemically (Fig. 2). We also found that membrane targeting of NEMO requires a motor protein, Myo1c (Fig. 3). Collectively, the data indicate the scaffold protein NEMO to be transported to membrane ruffles by the motor protein Myo1c. These observations are consistent with our aforementioned hypothesis.

Myo1c promotes IRS-1–IKK interaction and mediates Ser^{307} phosphorylation on IRS-1

A recent study showed that IKKs interact with IRS-1 and interfere with insulin signaling (Gao et al., 2002). To confirm this interaction in culture adipocytes, we first examined the localization of endogenous NEMO and IRS-1 (Fig. 4 A) or Xpress-tagged NEMO and eGFP-tagged IRS-1 (Fig. 4, B and C). In the basal state, IRS-1 was present in the cytoplasm, whereas with insulin stimulation, IRS-1 and NEMO colocalized to discrete foci in the cytoplasm as well as membrane ruffles. These observations on the intracellular localization of IRS-1 were very similar to those described in a study by Luo et al. (2005). They reported a mechanism of IRS-1 signal down-regulation involving the formation of a sequestration complex containing IRS-1 in

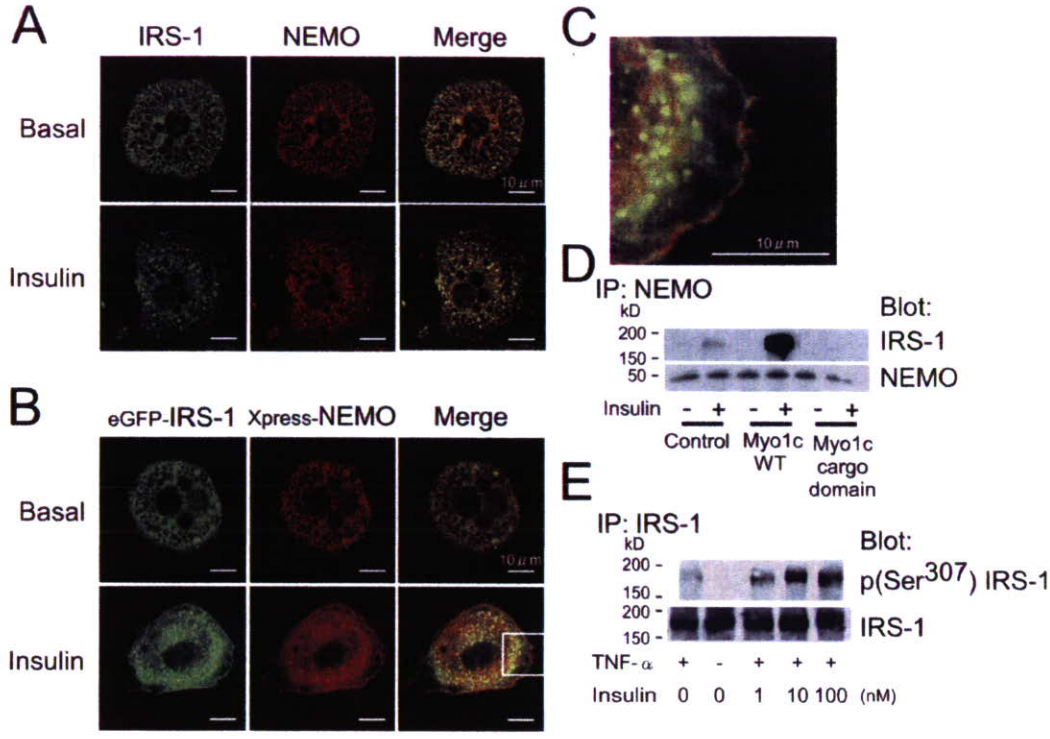

Figure 4. **Myo1c modulates IRS-1–NEMO interaction.** (A) 3T3-L1 adipocytes were serum starved for 2 h and stimulated with or without 100 nM insulin for 15 min at 37°C. Cells were fixed and stained with anti–IRS-1 and anti-NEMO antibody followed by FITC and Cy3-labeled secondary antibodies. (B) eGFP-tagged IRS-1 and Xpress-fused NEMO were coexpressed in 3T3-L1 adipocytes. After 2 h of serum starvation, the cells were stimulated with or without 100 nM insulin for 15 min and were then fixed. Expressed NEMO was visualized by anti-Xpress antibody and a Cy3-labeled second antibody. (C) High resolution view of the boxed area outlined in B. (D) 3T3-L1 adipocytes were infected with adenovirus encoding WT Myo1c and dominant inhibitory Myo1c. The cells were stimulated with or without 100 nM insulin for 15 min. The cell lysates were immunoprecipitated with anti-NEMO antibody, and precipitates were immunoblotted with anti–IRS-1 antibody. (E) 3T3-L1 adipocytes were left untreated or treated with 20 ng/ml TNF-α for 10 min and were incubated with various concentrations (1–100 nM) of insulin for 10 min at 37°C. The cells were lysed and immunoprecipitated by anti–IRS-1 antibody, and the precipitates were blotted with antiphospho-Ser^{307} IRS-1 and anti–IRS-1 antibody.

CHO-K1 cells. Interestingly, the large intracellular IRS-1 complexes (foci) appeared to be the negative regulatory machinery.

We next examined the direct interaction between endogenous IRS-1 and NEMO by immunoprecipitation (Fig. 4 D). Interestingly, the overexpression of Myo1c markedly increased this interaction. In contrast, cells overexpressing the dominant inhibitory cargo domain of Myo1c showed a diminished interaction. One interpretation of these findings is that Myo1c mediates the interaction by delivering NEMO to IRS-1. This explanation is supported by another set of experiments shown in Fig. S2 (A and B; available at http://www.jcb.org/cgi/content/full/jcb.200601065/DC1). These experiments focused on Myo1c–IKK-β and IRS-1–IKK-β associations. When NEMO was knocked down, the Myo1c–IKK-β interaction was disturbed. Similarly, the overexpression of ΔN-NEMO (detailed in the next section) diminished the IRS-1–IKK-β interaction. These results, combined with the data shown in Fig. 3, are consistent with our hypothesis that Myo1c transports the IKK complex via binding to NEMO.

Another interesting observation illustrated in Fig. 4 D was that insulin enhanced the association between IRS-1 and IKK-β. These data raise the possibility that insulin may assemble clusters of signaling molecules to facilitate the interaction between IKKs and IRS-1. To assess this possible new role of insulin, we performed two additional experiments. First, we observed IRS-1 Ser^{307} phosphorylation induced by TNF-α after treatment with various concentrations of insulin (Fig. 4 E). Although TNF-α–induced serine phosphorylation of IRS-1 was detected within 20 min even in the absence of insulin, a low concentration of insulin markedly enhanced TNF-α–induced Ser^{307} phosphorylation. These data are consistent with the results presented in Fig. 4 D. Next, we also observed Ser^{307} phosphorylation of IRS-1 in adipocytes expressing WT Myo1c and dominant inhibitory Myo1c. Overexpression of dominant inhibitory Myo1c diminished Ser^{307} phosphorylation of IRS-1 (Fig. S3 A, available at http://www.jcb.org/cgi/content/full/jcb.200601065/DC1). These results show that Myo1c promotes the interaction between IRS-1 and NEMO and mediates Ser^{307} phosphorylation of IRS-1. Furthermore, a low dose of insulin and an intact actin cytoskeleton may be necessary for clustering molecules related to TNF-α to down-regulate IRS-1.

Effects of NEMO and Myo1c expression on insulin signaling and glucose transport

Because IRS-1 protein is a key mediator of insulin signaling, we next focused on the roles of Myo1c and NEMO in insulin signaling and glucose transport. We prepared WT NEMO and NH_2-terminal–deleted (ΔN; residues 101–412) NEMO constructs

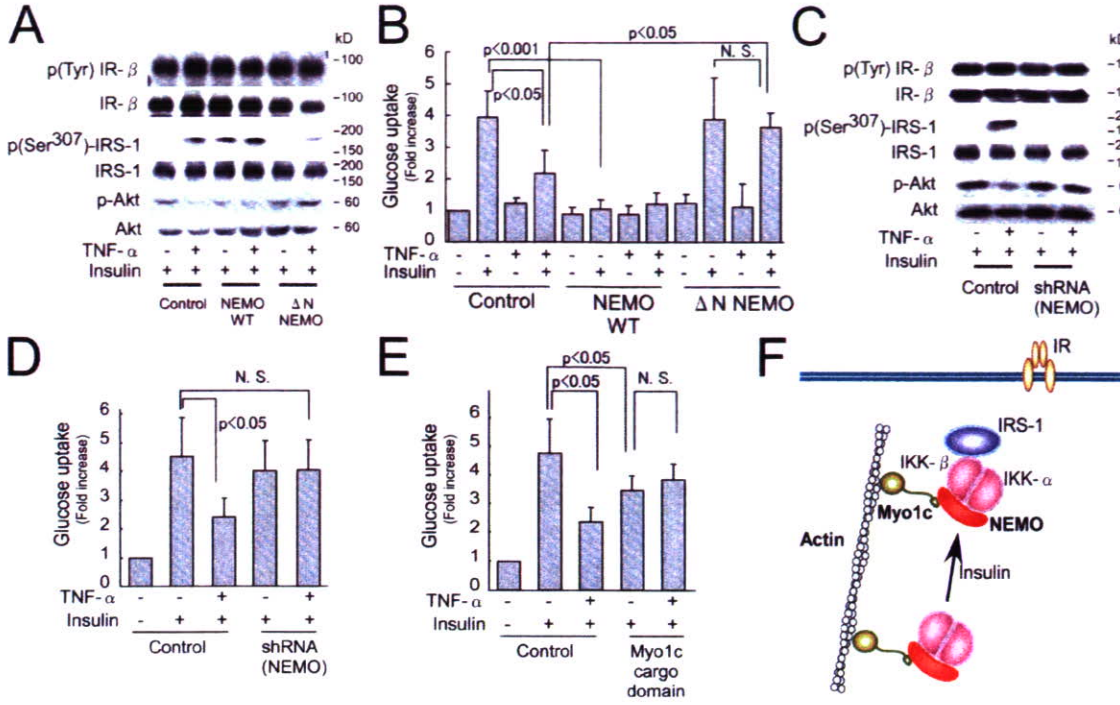

Figure 5. **NEMO and Myo1c for insulin signaling and glucose uptake in 3T3-L1 adipocytes.** (A–E) 3T3-L1 adipocytes were infected with recombinant adenovirus encoding wild type (WT) NEMO, ΔN-NEMO, shRNA (NEMO), Myo1c WT, Myo1c cargo domain, and vector alone (for control) at an MOI of 50. (A and C) The cells were serum starved for 2 h, treated with or without 20 ng/ml TNF-α for 15 min, and stimulated with or without 100 nM insulin for 10 min at 37°C. The cell lysates were immunoprecipitated with anti–insulin receptor β (IR-β) or anti–IRS-1 antibody, and the precipitates were immunoblotted with antiphosphotyrosine, anti–IR-β, anti–IRS-1, antiphospho-Ser^{307} IRS-1, antiphospho-Ser^{473} Akt, and anti-Akt antibodies. (B, D, and E) The cells were serum starved for 2 h in Krebs-Ringer phosphate buffer and treated with 20 ng/ml TNF-α for 4 h. Glucose uptake was measured. Each bar represents the mean ± SD (error bars) value of at least three independent experiments. (F) Schematic model of Myo1c-mediated IRS-1–IKK complex formation.

and performed a series of experiments. The NH_2 terminal of NEMO is the IKK-β–binding site, and deletion of this site was shown to impair the binding of NEMO with IKK-β (Yamamoto et al., 2001).

First, we assessed the effects of NEMO expression on upstream insulin signal cascades in 3T3-L1 adipocytes. Overexpression of WT NEMO induced the phosphorylation of IRS-1 Ser^{307} while decreasing Akt phosphorylation in the absence of TNF-α. Overexpression of ΔN-NEMO prevented the phosphorylation of IRS-1 Ser^{307} and inhibited Akt phosphorylation. We detected no changes in the tyrosine phosphorylation of the IR β chain (Fig. 5 A). Second, we measured 2-deoxyglucose uptake in 3T3-L1 adipocytes expressing NEMO constructs. Overexpression of WT NEMO abolished insulin-stimulated glucose uptake in the absence of TNF-α. In contrast, the overexpression of ΔN-NEMO completely blocked the inhibitory effects of TNF-α (Fig. 5 B). Third, we introduced shRNA into culture adipocytes to induce specific degradation of NEMO mRNA. NEMO protein expression was decreased to 20–30% of the control level (unpublished data). As expected, the deletion of NEMO almost completely blocked the inhibition of insulin-stimulated glucose uptake by TNF-α (Fig. 5 D). Under these conditions, IR-β tyrosine, IRS-1 Ser^{307}, and Akt Ser^{473} phosphorylations were examined in 3T3-L1 adipocytes. NEMO silencing by shRNA also prevented TNF-α–mediated IRS-1 Ser^{307} phosphorylation and inhibition of Akt phosphorylation without affecting IR tyrosine phosphorylation (Fig. 5 C). These data, combined with the data presented in Figs. 3 and 4, suggest that motor protein Myo1c and its receptor protein NEMO mediate TNF-α–induced down-regulation of IRS-1 and glucose uptake.

However, it was previously shown that the overexpression of ΔN-NEMO results in the loss of IKK kinase activity (Yamamoto et al., 2001). We confirmed the inhibition of IKK kinase activity in 3T3-L1 adipocytes expressing ΔN-NEMO as well as NEMO knockdown cells (Fig. S3, B and C). These observations indicated that NEMO plays a role in assembling the IKK complex and that this step is critical for IKK kinase activity. To avoid this bias and clarify the roles of Myo1c and NEMO in glucose uptake, we conducted another experiment using Myo1c cargo domain constructs. As shown in Fig. 5 E, overexpression of the cargo domain inhibited the TNF-α–induced suppression of glucose uptake. Together, these results provide evidence that NEMO may function as a receptor molecule for Myo1c and that Myo1c promotes the TNF-α–induced suppression of metabolic insulin action. In agreement with a previous study (Bose et al., 2002), we confirmed that Myo1c cargo domain expression itself decreased insulin-stimulated glucose uptake by 30%. This may be a result of the inhibitory role of Myo1c on GLUT4 recycling (Bose et al., 2002).

Based on the aforementioned data, we propose a simple model whereby Myo1c and its receptor NEMO cooperatively facilitate IKK–IRS-1 complex formation, as illustrated in Fig. 5 F. NEMO is a scaffold protein of the IKK complex. Recent studies suggest that some scaffold proteins serve as links between

molecular motors and intracellular vesicles, thereby functioning as cargo proteins (Dorner et al., 1999; Setou et al., 2000). In contrast, our data suggest that the scaffold protein NEMO links motor and signaling molecules as cargos. It is noteworthy that Myo1c organizes the signaling complex and serves as a platform for the two distinct signals to interact (i.e., the insulin signal and the TNF-α signal mediating insulin resistance).

Finally, our results allow us to draw three conclusions. First, the motor protein Myo1c appears to participate directly in the mechanism of IRS-1–IKK complex formation in culture adipocytes. It is possible that NEMO is a molecular receptor linking motor (Myo1c) and cargo (IKK-α and -β). Second, NEMO and Myo1c may be involved in the TNF-α–induced Ser^{307} phosphorylation of IRS-1, resulting in the attenuation of insulin signaling and glucose transport. Third, Myo1c and the actin cytoskeleton may facilitate formation of the signaling molecule complex that participates in the TNF-α–induced down-regulation of IRS-1. In summary, our data suggest that Myo1c and NEMO are responsible for the mechanism of TNF-α–induced insulin resistance.

Materials and methods

Constructs

Mouse full-length NEMO and IRS-1 were cloned by RT-PCR amplification with total mRNA from 3T3-L1 adipocytes. WT and an NH_2-terminal deletion mutant of NEMO containing amino acid residues 101–412 were subcloned into pEGFP-C2, pcDNA3.1His, pET-16b, and/or pGEX-6p-1 vectors. Mouse Myo1c cDNA was purchased from DNAFORM and subcloned into p3xFLAG-CMV7.1, pET-16b, and pGEX-6p-1 vectors. IKK-α and IKK-β cDNA were gifts from H. Nakano (Juntendo University School of Medicine, Tokyo, Japan).

Reagents and antibodies

The following antibodies were used: anti-NEMO, antiphospho-Ser^{307} IRS-1, and antiphospho-Akt antibodies (Cell Signaling); anti-NEMO and anti–IRS-1 antibodies (Upstate Biotechnology); anti-Flag antibody (Sigma-Aldrich); anti-Xpress antibody (Invitrogen); and Cy3-conjugated anti–mouse IgG (Jackson ImmunoResearch Laboratories). Rabbit polyclonal anti-Myo1c antibody was generated against the peptide sequence DKSELSDKKRPE. All other antibodies were purchased from Santa Cruz Biotechnology, Inc. AlexaFluor596-phalloidin was obtained from Invitrogen. Mouse TNF-α was purchased from PeproTech.

Cell culture

3T3-L1 fibroblasts were grown in DME with 10% FBS at 37°C. The cells (3–4-d after confluence) differentiated into adipocytes with incubation in the same DME containing 0.5 mM isobutylmethylxanthine, 0.25 μM dexamethasone, and 4 μg/ml insulin for 3 d and were then grown in DME with 10% FBS for an additional 3–6 d.

Immunofluorescence microscopy and digital image analysis

Differentiated 3T3-L1 adipocytes were transfected by electroporation. The cells were then replated onto coverslips and allowed to recover for 48 h followed by stimulation with 100 nM insulin or 20 ng/ml TNF-α for 15 min at 37°C. Then, 5 μM latrunculin B or 30 μM nocodazole were added 60 min before treatment with insulin. Minimum concentrations of these agents required for disrupting the cytoskeleton in culture adipocytes were determined previously (Emoto et al., 2001). Cells were fixed with 3.7% formaldehyde in PBS, permeabilized with buffer A (0.5% Triton X-100 and 1% FBS in PBS) for 15 min, and incubated for 2 h with primary antibodies at room temperature. The cells were washed and incubated with an appropriate secondary antibody or AlexaFluor596-phalloidin for 30 min. The coverslips were washed thoroughly and mounted on glass slides. Immunostained cells were observed at room temperature with a laser-scanning confocal microscope (LSM5 PASCAL; Carl Zeiss MicroImaging, Inc.) and its two-channel scanning module equipped with an inverted microscope (Axiovert 200M; Carl Zeiss MicroImaging, Inc.). The inverted microscope used the 63× NA 1.4 oil objective lens run by LSM5 processing software (Carl Zeiss MicroImaging, Inc.) and Adobe Photoshop CS2.

Preparation of adenovirus

Adenovirus producing mouse WT NEMO, deletion mutant NEMO (residues 101–412), mouse WT Myo1c, and dominant inhibitory Myo1c (residues 767–1,028) were prepared using an AdEasy Adenoviral Vetor System (Stratagene).

shRNA-induced degradation of NEMO

shRNA was designed to have a 5′-AAGGATTCGAGCAGTTAGTGAGC-3′ sequence. Synthetic complementary single-stranded oligonucleotide DNA was annealed, and the double-stranded DNA of the target sequence was created. This annealed DNA was inserted into a pcPUR+U6i cassette (Miyagishi and Taira, 2002), and the insert was transferred to an AdEasy Adenoviral Vector System. This shRNA system decreased NEMO protein expression to 20–30% of the control level.

Identification of NEMO-binding proteins

Myc-NEMO was expressed in 3T3-L1 adipocytes. 2 d thereafter, cells were serum starved for 2 h and stimulated with 100 nM insulin or 20 ng/ml TNF-α for 20 min. Cell lysates were prepared and immunoprecipitated with anti-myc antibody. Samples were resolved by SDS-PAGE, and proteins were visualized by silver staining. The bands were excised and subjected to in-gel digestion according to the method described by Shevchenko et al. (1996) with minor modifications. Mass spectra were acquired using a time of flight mass spectrometer (Voyager DE Pro; Applied Biosystems). The search engine for the peptide mass fingerprint was the web-based Mascot (Matrix Science).

Details of in-gel digestion. In brief, the gel pieces were washed twice in 300 μl CH_3CN for 30 min and dried. The gel pieces were then rehydrated in 100 μl of reduction buffer (10 mM DTT and 100 mM NH_4HCO_3) and were left standing at 56°C for 1 h. After supernatant removal, the gel pieces were incubated in 100 μl of 50 mM idotoacetamide in 100 mM NH_4HCO_3 for 45 min at room temperature. The gel pieces were then washed in 100 μl of 100 mM NH_4HCO_3 and dehydrated in 300 μl of acetonitrile. After washing and dehydration (twice each), the dried gel pieces were rehydrated on ice in 100 μl of digestion buffer (50 mM NH_4HCO_3 and 12.5 ng/μL each of lysylendopeptidase [Wako] and sequencing grade trypsin [Promega]) for 45 min. The supernatant was replaced with 50 mM NH_4HCO_3, and the gel pieces were incubated at 37°C overnight. The supernatant was collected, and the peptides were extracted repeatedly with a 50-μl solution of 5% (vol/vol) formic acid and 50% (vol/vol) acetonitrile by vortexing. The combined supernatants were evaporated to dryness in a vacuum centrifuge. Resulting peptides were redissolved in 0.1% trifluoroacetic acid and absorbed onto ZipTip C18 (Millipore). Bound peptides were eluted with 50% acetonitrile and 0.1% trifluoroacetic acid. Equal amounts of the resulting peptide solution and a matrix-assisted laser desorption ionization sample matrix solution (10 mg/ml α-cyano-4-hydroxycinnamic acid dissolved in 50% acetonitrile and 0.1% trifluoroacetic acid) were mixed on the sample target.

Pull-down assay

GST-fused NEMO and Myo1c were expressed using a pGEX-6p-1 vector in BL21 cells. His-tagged NEMO and Myo1c were expressed using a pET-16b vector in BL21 (DE3) cells. GST-fused protein and His-tagged protein were mixed in PBS and pulled down with glutathione–Sepharose beads (GE Healthcare). Protein interactions were detected by Western blotting using anti-His antibody and anti-GST antibody.

shRNA-induced degradation of Myo1c

Target sequences used in shRNA were the same as those described previously (Bose et al., 2002). Synthetic complementary single-stranded oligonucleotide DNAs were annealed to make double-stranded DNAs of the target sequences. These annealed DNA were inserted into a pcPUR+U6i cassette vector, and the plasmids were electroporated into differentiated 3T3-L1 adipocytes.

Immunoprecipitation and immunoblotting

Cells were lysed in lysis buffer (20 mM Hepes, pH 7.2, 100 mM NaCl, 1 mM EDTA, 25 mM NaF, 1 mM sodium vanadate, 1 mM benzamidine, 5 μg/ml leupeptin, 5 μg/ml aprotinin, 1 mM PMSF, and 1 mM DTT), and the protein concentration was measured with bicinchoninic acid protein assay reagent (Pierce Chemical Co.). For immunoprecipitation, the cell lysate was preincubated with protein G–Sepharose beads at 4°C for 30 min